Table 1. Effects of Various Ligands on *in Vitro* [^{11}C]**2** Binding to Rat Brain Slices

Ligands		% control binding in frontal cortex[a]		
		10 μM	100 μM	1 mM
Unlabelled compd	**2**	69.3	47.7	
Polyamine site				
Agonists	Spermine		64.1	43.2
	Spermidine		89.5	46.3
	Putrescine		98.8	84.6
Antagonists	CP-101,606	81.1	71.1	
	Ifenprodil	67.2	59	
Glutamate site				
Agonist	Glutamate			102.2
Antagonist	CGS-19755		96	
Glycine site				
Agonist	Glycine			100.8
Antagonist	DCKA		108.4	
Divalent catons				
	$MgCl_2$		93.3	65.2
	$CaCl_2$		91.6	63.2
	$Zn(OAc)_2$		45.1	26.7
Ion channel site				
Antagonist	MK-801		88.3	
Others receptors				
α1	Prazosin		99.4	
σ1, 2	DTG		90.4	
5-HT1a	8-OH-DPAT		58.9	
5-HT2	Ketanserin		68.8	

a) Average values obtained by at least triplicate from three S.D. rats.

Table 2. Effects of Various Ligands on *in Vitro* [^{11}C]**3** Binding to Rat Brain Slices

Ligands		% control binding in frontal cortex[a]		
		10 μM	100 μM	1 mM
Unlabelled compd	**3**	79.5	63.3	
Polyamine site				
Agonists	Spermine		61.4	49
	Spermidine		88.3	67.6
	Putrescine		105.4	88.3
Antagonists	CP-101,606	94.1	99.2	
	Ifenprodil	83.1	71.9	
Glutamate site				
Agonist	Glutamate			102.8
Antagonist	CGS-19755		114.5	
Glycine site				
Agonist	Glycine			103.7
Antagonist	DCKA		100.4	
Divalent cations				
	$MgCl_2$		94.9	76.4
	$CaCl_2$		96.3	66.3
	$Zn(OAc)_2$		69.7	33.8
Ion channel site				
Antagonist	MK-801		104.3	
Other receptors				
α1	Prazosin		94.2	
σ1, 2	DTG		101.7	
5-HT1a	8-OH-DPAT		97.9	
5-HT2	Ketanserin		93.8	

a) Average values obtained by at least triplicate from three S.D. rats.

served in the *in vitro* binding of ifenprodil-like NR2B-selective drugs.[10,25,35] Glutamate, glycine , glutamate site antagonist CGS-19755, glycine site antagonist DCKA and channel site antagonist MK-801, had no inhibitory effect on either [^{11}C]**2** or [^{11}C]**3** binding even at high concentrations. The serotonergic receptor ligands, 8-OH-DPAT and ketanserin, showed 30—40% inhibition toward the binding of [^{11}C]**2** at concentrations of 100 μM, whereas no inhibition of [^{11}C]**3** was observed with these ligands at the same concentrations, suggesting that the binding of [^{11}C]**2** was also occurring at the serotonin recognition sites. As shown in Figs. 2 and 3, taking into account the bindings of the radioligands to the cerebellum, a region free of the NR2B subunit, it seems likely that these radioligands bind to the spermine- and/or ifenprodil-binding sites unrelated to the NR2B subunit. Our efforts to determine the IC_{50} value from inhibition studies using rat brain slices have not been successful because of high nonspecific binding fractions, but bis(phenylalkyl)-amine **2** and **3** are estimated to have moderate affinities to the spermine- and/or ifenprodil-binding sites.

From these *in vitro* results, [^{11}C]**3** was chosen for further evaluation under *in vivo* conditions because of its greater selectivity for the spermine- and/or ifenprodil-binding sites than [^{11}C]**2**. The brain regional distribution of [^{11}C]**3** after intravenous injection was investigated using mice. As shown in Table 3, [^{11}C]**3** showed an initial moderate brain uptake (0.8—0.9% dose/g) and increased slightly with time. The radioactivity levels of blood were lower than those in the brain. No significant difference in the regional brain distribution was observed, similar to the *in vitro* brain distribution.

Furthermore, we evaluated the effect of pre-treatment with

Table 3. Biodistribution of [^{11}C]**3** in Mouse Brain and Blood

Tissue	% dose/g (mean ± S.D.)[a]		
	10 min	30 min	50 min
Blood	0.74±0.12	0.61±0.05	0.68±0.06
Cerebral cortex	0.89±0.15	1.07±0.05	1.11±0.15
Striatum	0.86±0.19	0.95±0.05	1.07±0.18
Hippocampus	0.74±0.12	0.95±0.01	0.90±0.13
Cerebellum	0.87±0.16	0.93±0.01	0.95±0.13

a) Average of three mice.

spermine or with non-radioactive **3** on brain uptake using rats. As shown in Fig. 4, pre-treatment with non-radioactive **3** (7 μmol/kg) caused a statistically significant increase of radioactivity in the cerebral cortex and hippocampus compared with the control group. The reasons for this observation are uncertain in the present study. However, it is likely that the binding of [^{11}C]**3** in peripheral binding sites or to plasma proteins might be prevented, resulting in an increased availability for uptake in the brain. Thus, this pre-treatment with unlabelled **3** suggests that the uptake observed is nonspecific in nature. Pre-treatment with spermine (7 μmol/kg) did not produce any change of uptake in the brain compared to the control. This finding is in contrast to the *in vitro* inhibition of [^{11}C]**3** binding on brain slices. The insensitivity of a blocking effect by exogenously administered spermine is probably due to the low penetration of spermine across the blood-brain barrier,[36] and it is also feasible that a high concentration of endogenous polyamines, such as spermine, in the central nervous system would behave as an endogenous inhibitor for [^{11}C]**3** binding *in vivo*. Recently it has been proven that the

glycine-site antagonist, [^{11}C]L-703,717, is susceptible to inhibition by the endogenous amino acids glycine and D-serine in its *in vivo* binding.[37] Thus ,we could not prove that the brain accumulation of [^{11}C]**3** was due to the binding of the ligand to spermine- and/or ifenprodil-binding sites.

In vivo brain distribution of [^{11}C]**3** was further assessed by a conscious Rhesus monkey in conjunction with PET. Figure 5 shows the normalized time activity curves in the frontal and occipital cortex, and cerebellum for 90 min of PET scanning after intravenous injection of [^{11}C]**3**. The radioactivity reached maximal values at 20—30 min and then decreased slightly until the end of the experiments. No significant regional differences in uptake of radioactivity were observed, similar to what we obtained using mouse and rat brains, as described above. When unlabelled **3** (6 μmol/kg) was co-injected with [^{11}C]**3**, a slight decrease in brain radioactivity that was most apparent at later time-points, was induced as shown in Fig. 5, seemingly indicating that there is a small fraction of displaceable binding in these regions of monkey brain. Additional experiments are, however, necessary to more precisely reveal the specific binding sites of [^{11}C]**3** *in vivo*.

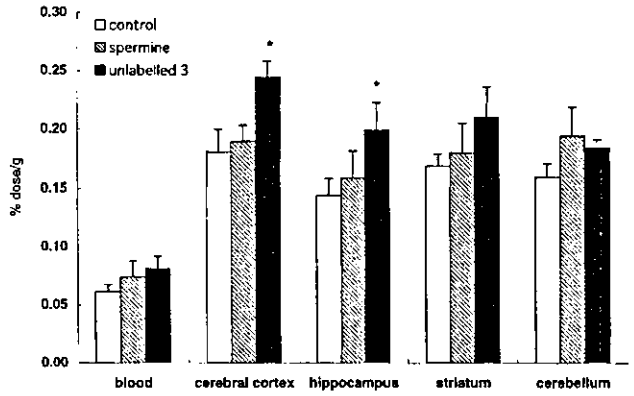

Fig. 4. Effects of Pretreatment with Spermine and Unlabelled **3** in the Brain Uptake of [^{11}C]**3** in Rats

Spermine (7 μmol/kg) or unlabelled **3** (7 μmol/kg) was injected intravenously 10 min before injection of [^{11}C]**3**. Rats were killed at 30 min after injection of [^{11}C]**3**. *Significant difference ($p<0.05$) *versus* the corresponding value of the control by two way ANOVA followed by Turkey's test.

The new radiolabelled ligands, ^{11}C-labelled bis(phenylpropyl)amine ([^{11}C]**2**) and bis(phenylbutyl)amine ([^{11}C]**3**), were designed based on bis(phenylalkyl)amines (**1**) which have been reported as polyamine site antagonists with high selectivity for NR1A/2B NMDA receptors. However, *in vitro* competitive experiments show that [^{11}C]**2** and [^{11}C]**3** share the binding sites with spermine and/or ifenprodil but not with CP-101,606, a highly potent NR2B-selective NMDA antagonist, and that [^{11}C]**2** has, additionally, appreciable affinity for the serotonergic receptors. Polyamines such as spermine and spermidine are present in cells at high concentrations and the NMDA receptors contain multiple binding sites for them. Ifenprodil binds at two sites on NMDA receptors, together with three binding sites on other proteins. Such multiplicity of binding sites of spermine and ifenprodil may be responsible for high ratio of nonspecific binding of [^{11}C]**3** *in vivo*. In addition, endogenous divalent cations, as well as endogenous polyamines, seem likely to affect the *in vivo* [^{11}C]**3** binding. Both [^{11}C]**2** and [^{11}C]**3** are therefore not suitable radioligands for PET imaging of brain binding sites on

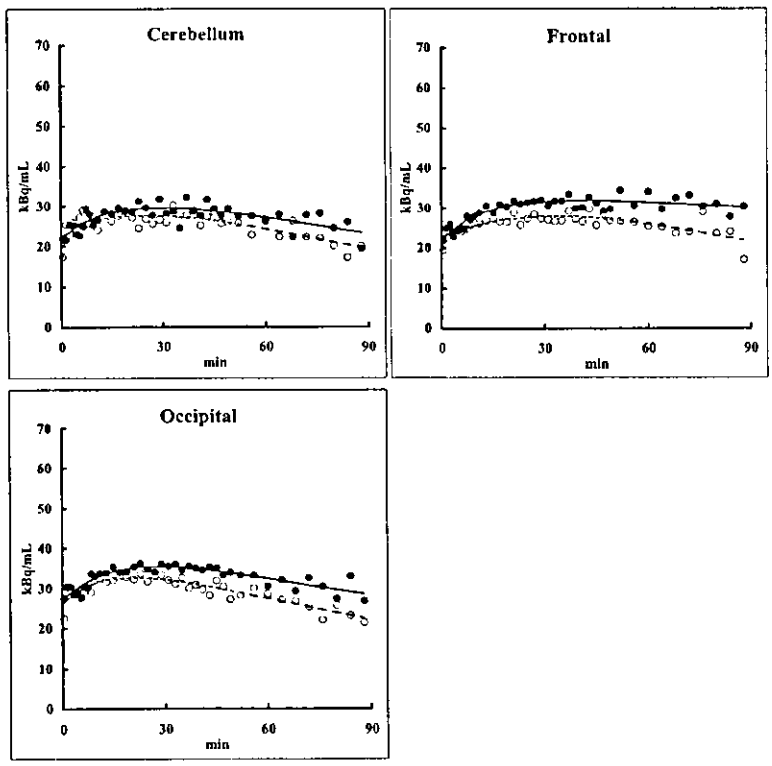

Fig. 5. Time-Activity Curves in the Cerebellum, Frontal Cortex and Occipital Cortex of Monkey Brain Obtained by PET

Each point was normalized to the injected dose of 185 MBq. Control (closed circles) and co-treatment (open circles) with 6 μmol·kg of unlabelled **3**.

the NMDA receptors.

Acknowledgements We are grateful to Mr. Toshihiko Henmi for his support in ^{11}C-methylation. We thank the cyclotron crew of the National Institute of Radiological Sciences for their help in the ^{11}C production in this work. This work has been supported in part by CREST, Japan Science and Technology Corporation.

REFERENCES

1) Choi D. W., *Neuron*, **1**, 623—634 (1988).
2) Dewar D., Chalmers D. T., Shand A., Graham D. I., McCulloch J., *Ann. Neurol.*, **28**, 805—810 (1990).
3) Johnson R. L., Koerner J. F., *J. Med. Chem.*, **31**, 2057—2066 (1988).
4) Ouyang X., Mukherjee J., Yang Z., *Nucl. Med. Biol.*, **23**, 315—324 (1996).
5) Patel S., Chapman A. G., Graham J. L., Meldrum B. S., Frey P., *Epilepsy Res.*, **17**, 3—10 (1990).
6) Rothman S. M., Olney J. W., *Trends Neurosci.*, **18**, 57—58 (1995).
7) Stone T. W., Burton N. R., *Prog. Neurobiol.*, **30**, 333—368 (1988).
8) Young A. B., Greenamyre J. T., Hollingsworth Z., Albin R., D'Amato C., Shoulson I., Penney J. B., *Science*, **241**, 981—983 (1988).
9) Bressan R. A., Pilowsky L. S., *Eur. J. Nucl. Med.*, **27**, 1723—1731 (2000) and references cited therein.
10) Dingledine R., Borges K., Bowie D., Traynelis S. F., *Pharmacol. Rev.*, **51**, 7—61 (1999).
11) Loftis J. M., Janowsky A., *Pharmacol. Ther.*, **97**, 55—85 (2003).
12) Kutsuwada T., Kashiwabuchi N., Mori H., Sakimura K., Kushiya E., Araki K., Meguro H., Masaki H., Kumanishi T., Arakawa M., Mishina M., *Nature* (London), **358**, 36—41 (1992).
13) Monyer H., Sprengel R., Schoepfer R., Herb A., Higuchi M., Lomeli H., Burnashev N., Sakmann B., Seeburg P. H., *Science*, **256**, 1217—1221 (1992).
14) Moriyoshi K., Masu M., Ishii T., Shigemoto R., Mizuno N., Nakanishi S., *Nature* (London), **354**, 31—37 (1991).
15) Tamiz A. P., Whittemore E. R., Zhou Z. L., Huang J. C., Drewe J. A., Chen J. C., Cai S. X., Weber E., Woodward R. M., Keana J. F., *J. Med. Chem.*, **41**, 3499—3506 (1998).
16) Benveniste M., Mayer M. L., *J. Physiol.*, **464**, 131—163 (1993).
17) Lerma J., *Neuron*, **8**, 343—352 (1992).
18) McGurk J. F., Bennett M. V., Zukin R. S., *Proc. Natl. Acad. Sci. U.S.A.*, **87**, 9971—9974 (1990).
19) Rock D. M., MacDonald R. L., *Mol. Pharmacol.*, **41**, 83—88 (1992).
20) Rock D. M., MacDonald R. L., *Mol. Pharmacol.*, **42**, 157—164 (1992).
21) Sacaan A. I., Johnson K. M., *Mol. Pharmacol.*, **36**, 836—839 (1989).
22) Williams K., Dawson V. L., Romano C., Dichter M. A., Molinoff P. B., *Neuron*, **5**, 199—208 (1990).
23) Williams K., Zappia A. M., Pritchett D. B., Shen Y. M., Molinoff P. B., *Mol. Pharmacol.*, **45**, 803—809 (1994).
24) Suzuki K., Inoue O., Hashimoto K., Kuchiki M., Tamate K., *Appl. Radiat. Isot.*, **36**, 971—976 (1985).
25) Haradahira T., Maeda J., Okauchi T., Zhang M. R., Hojo J., Kida T., Arai T., Yamamoto F., Sasaki S., Maeda M., Suzuki K., Suhara T., *Nucl. Med. Biol.*, **29**, 517—525 (2002).
26) Sihver S., Sihver W., Bergsrom M., Hoglund U., Sjoberg P., Langstrom B., Watanabe Y., *J. Pharmacol. Exp. Ther.*, **290**, 917—922 (1999).
27) Okauchi T., Suhara T., Maeda J., Kawabe K., Obayashi S., Suzuki K., *Synapse*, **41**, 87—95 (2001).
28) Chenard B. L., Shalaby I. A., Koe B. K., Ronau R. T., Butler T. W., Prochniak M. A., Schmidt A. W., Fox C. B., *J. Med. Chem.*, **34**, 3085—3090 (1991).
29) Karbon E. W., Patch R. J., Pontecorvo M. J., Ferkany J. W., *Eur. J. Pharmacol.*, **176**, 247—248 (1990).
30) Dana C., Benavides J., Schoemaker H., Scatton B., *Neurosci. Lett.*, **125**, 45—48 (1991).
31) Hashimoto K., Mantione C. R., Spada M. R., Neumeyer J. L., London E. D., *Eur. J. Pharmacol.*, **266**, 67—77 (1994).
32) Menniti F., Chenard B., Collins M., Ducat M., Shalaby I., White F., *Eur. J. Pharmacol.*, **331**, 117—126 (1997).
33) Schoemaker H., Allen J., Langer S. Z., *Eur. J. Pharmacol.*, **176**, 249—250 (1990).
34) Williams K., *Mol. Pharmacol.*, **44**, 851—859 (1993).
35) Mutel V., Buchy D., Klingelschmidt A., Messer J., Bleuel Z., Kemp J. A., Richards J. G., *J. Neurochem.*, **70**, 2147—2155 (1998).
36) Shin W. W., Fong W. F., Pang S. F., Wong P. C. L., *J. Neurochem.*, **44**, 1056—1059 (1985).
37) Haradahira T., Okauchi T., Maeda J., Zhang M. R., Nishikawa T., Konno R., Suzuki K., Suhara T., *Synapse*, **50**, 130—136 (2003).

SYNAPSE 52:283–291 (2004)

Novel Peripheral Benzodiazepine Receptor Ligand [^{11}C]DAA1106 for PET: An Imaging Tool for Glial Cells in the Brain

JUN MAEDA,[1,2] TETSUYA SUHARA,[1,2*] MING-RONG ZHANG,[3,4] TAKASHI OKAUCHI,[1,2] FUMIHIKO YASUNO,[1,2] YOKO IKOMA,[1] MOTOKI INAJI,[1] YUJI NAGAI,[1,2] AKIHIRO TAKANO,[1,2] SHIGERU OBAYASHI,[1,2] AND KAZUTOSHI SUZUKI[3]

[1]*Brain Imaging Project, National Institute of Radiological Sciences, Chiba, Japan*
[2]*CREST, Japan Science and Technology Corporation (JST), Saitama, Japan*
[3]*Department of Medical Imaging, National Institute of Radiological Sciences, Chiba, Japan*
[4]*SHI Accelerator Service Ltd., Tokyo, Japan*

KEY WORDS peripheral benzodiazepine receptor; positron emission tomography; DAA1106; PK11195; microglia

ABSTRACT Peripheral benzodiazepine receptor (PBR) is expressed in most organs and its expression is reported to be increased in activated microglia in the brain. [^{11}C]PK11195 has been widely used for the in vivo imaging of PBRs, but its signal in the brain was not high enough for stable quantitative analysis. We synthesized a novel positron emission tomography (PET) ligand, [^{11}C]DAA1106, for PBR and investigated its in vivo properties in rat and monkey brain. High uptake of [^{11}C]DAA1106 was observed in the olfactory bulb and choroid plexus area, followed by the pons/medulla and cerebellum by in vivo autoradiography of rat brain, correlating with the binding in vitro. [^{11}C]DAA1106 binding was increased in the dorsal hippocampus with neural destruction, suggesting glial reaction. [^{11}C]DAA1106 binding was both inhibited and displaced by 1.0 mg/kg of DAA1106 and 5 mg/kg of PK11195 by 80% and 70%, respectively. Specific binding was estimated as 80% of total binding. [^{11}C]DAA1106 binding was four times higher compared to the binding of [^{11}C]PK11195 in the monkey occipital cortex. These results indicated that [^{11}C]DAA1106 might be a good ligand for in vivo imaging of PBR.
Synapse 52:283–291, 2004.

INTRODUCTION

Binding sites for benzodiazepine were initially identified by the binding of [^{3}H]diazepam not only in the brain but also in peripheral organs like kidney, liver, and lung (Braestrup and Squires, 1977; Squires and Braestrup, 1977). Benzodiazepine derivative Ro5-4864 binds only to peripheral binding sites with nanomolar affinity (Braestrup and Squires, 1977), and binding sites different from benzodiazepine binding sites on $GABA_A$ receptor were named peripheral benzodiazepine receptors (PBRs). PBR is primarily found on mitochondrial membranes in various peripheral tissues (Anholt et al., 1985, 1986; Antkiewicz-Michaluk et al., 1988a; Gavish et al., 1999). Although the term "peripheral" was widely used in the literature, specific ligands for PBR such as [^{3}H]Ro5-4864 and [^{3}H]PK11195 revealed that PBR was also expressed in the brain (Schoemaker et al., 1981; Benavides et al., 1983; Le Fur et al., 1983; Schoemaker et al., 1983). PK11195 binding in cultured microglia and astrocytes was at 8-fold higher density than in cultured neurons (Jayakumar et al., 2002), suggesting that PBRs localize in glial cells in the brain. The expression of PBR in vivo is reported to be increased in microglia activated by brain injury (Myers et al., 1991; Stephenson et al., 1995; Banati et al., 1997; Kuhlmann et al., 2002). PBR binding in the brain is highest in the olfactory bulb (Benavides et al., 1983; Schoemaker et al., 1983; Anholt et al., 1984; Cymerman et al., 1986), an area of dense microglia population (Caggiano and Brunjes, 1993).

Contract grant sponsor: PET project of the National Institute of Radiological Sciences, Chiba, Japan.

*Correspondence: Tetsuya Suhara, M.D. Ph.D., Brain Imaging Project, National Institute of Radiological Sciences, 9-1, Anagawa 4-Chome, Inage-ku, Chiba, 263-8555, Japan. E-mail: suhara@nirs.go.jp

Received 10 July 2003; Accepted 7 March 2004

DOI 10.1002/syn.20027

Published online 5 April 2004 in Wiley InterScience (www.interscience.wiley.com).

PBR is composed of at least three subunits: isoquinoline-binding protein (IBP) (Antkiewicz-Michaluk et al., 1988b; Sprengel et al., 1989; Parola et al., 1991), a voltage-dependent anion channel (VDAC), and an adenine nucleotide carrier (ANC) (McEnery et al., 1992). The trimeric complex is a critical component of the mitochondrial permeability transitional pore (MPTP), which plays an important role in the passage of various biogenic compounds between the cytoplasm and mitochondrial intermembrane or matrix (Casellas et al., 2002). A cholesterol-binding site was observed in the carboxyl terminus of IBP and the activation of PBR is suggested to be involved in the regulation of cholesterol transport into mitochondria and in steroidogenesis (Li et al., 2001).

[^{11}C]PK11195 is currently being used to visualize PBR in the brain, and especially for the evaluation of lesions, by positron emission tomography (PET) (Banati et al., 2000; Cagnin et al., 2001; Debruyne et al., 2002). [^{11}C]PK11195 binding was reported to be increased in the stroke region (Pappata et al., 2000), plaque of multiple sclerosis (Banati et al., 2000; Debruyne et al., 2002), the cortex of Alzheimer disease (Cagnin et al., 2001), and epileptic foci (Goerres et al., 2001). The mechanism of the increase in [^{11}C]PK11195 binding has been suggested as representing a reflection of activated microglia (Banati et al., 2000; Cagnin et al., 2001; Banati, 2002a,b). These reports suggested the diagnostic values of PBR in many disorders.

(*N*-5-fluoro-2-phenoxyphenyl)-*N*-(2,5-dimethoxybenzyl) acetamide (DAA1106) was originally developed as an anxiolytic with a different structure from other PBR compounds such as PK11195 and Ro5-4864 (Chaki et al., 1999; Okuyama et al., 1999; Okubo et al., 2004). The inhibition constant (K_i) of DAA1106 to [^{3}H]DAA1106 (0.043 nM) is one order smaller than that of PK11195 (0.77 nM), and it also has good selectivity for PBRs (Chaki et al., 1999). DAA1106 does not promote steroidogenesis in a mitochondrial fraction, suggesting that DAA1106 has an antagonistic property for PBRs (Culty et al., 2001). We have reported the synthesis of [^{11}C]DAA1106 and its high accumulation in the mouse brain (Zhang et al., 2003). The aim of this study was to characterize and evaluate [^{11}C]DAA1106 as a PET ligand for PBRs in the brains of rat and monkey.

MATERIALS AND METHODS

Synthesis of radiotracers

DAA1106 and DAA1123 (*N*-5-fluoro-2-phenoxyphenyl)-*N*-(2-hydroxy-5-methoxybenzyl) acetamide as desmethyl precursors were kindly donated by Taisho Pharmaceutical Co. (Tokyo, Japan). [^{11}C]CH_3I was transferred under a helium gas flow with heating into a reaction vessel containing anhydrous DMF (300 μl), DAA1123 (0.3–0.5 mg), and NaH (3–5 μl, 0.5 g/20 ml DMF) cooled to −15 to −20°C. After adding CH_3CN/H_2O (6/4, 500 μl), the radioactive mixture was applied to a semipreparative HPLC column (Zhang et al., 2003). The radioactive fraction corresponding to [^{11}C]-DAA1106 was collected in a sterile flask.

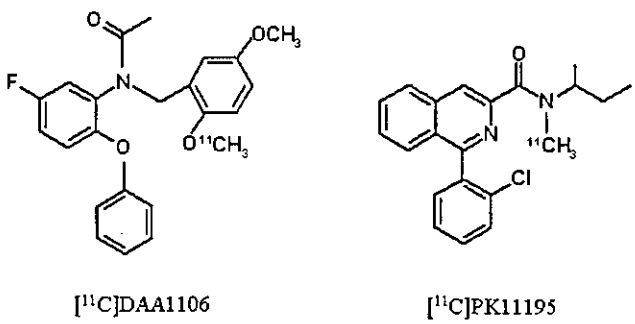

[^{11}C]DAA1106 [^{11}C]PK11195

Fig. 1. Chemical structure of two PBR tracers, [^{11}C]DAA1106 and [^{11}C]PK11195.

(R)-[^{11}C]PK11195 was synthesized by [^{11}C]-N-methylation of desmethyl precursor as previously described in detail (Hashimoto et al., 1989). The logP value of [^{11}C]PK11195 between octanol/phosphate buffer (pH 7.4) was determined by a shaken flask method as described in detail previously (Zhang et al., 2002).

The chemical structures of [^{11}C]DAA1106 and [^{11}C]PK11195 are shown in Figure 1. The specific radioactivity of [^{11}C]DAA1106 was 175 ± 78 GBq/μmol (mean ± SD; >60 GBq/μmol), and that of [^{11}C]-PK11195 was >74 GBq/μmol at the end of the synthesis. The tracer was injected into animals within 20 min following synthesis.

Animals

Male rats weighing 300–400 g and a male rhesus monkey (*Macaca mulatta*) weighing 7.0 kg were used. The animals were maintained and handled in accordance with recommendations by the US National Institutes of Health and our guidelines (National Institute of Radiological Sciences). The studies were approved by the Animal Ethics Committee of the National Institute of Radiological Sciences, Chiba, Japan.

Neural lesion of hippocampus

Rats were anesthetized with pentobarbital (60 mg/kg) and a cannula (Plastic One, Roanoke, VA) was implanted into the dorsal hippocampus (A/P −4.0 mm; L 2.5 mm, D/V 3.5 mm from bregma). Kainic acid (10 nmol in 5 μl of phosphate-buffered saline, pH 7.4) was infused into the right dorsal hippocampus for 5 min using a syringe-pump (BAS Instruments, West Lafayette, IN). Vehicle was injected into the left hippocampus as control. The rats were allowed to recover for 7 days before ex vivo or in vitro autoradiography. The uptake of [^{11}C]DAA1106 was evaluated by the ratio of the normal or lesioned hippocampus to the cerebral cortex. One-way ANOVA following post-hoc analysis with Scheffe's test was used for the evaluation.

Ex vivo autoradiography of [^{11}C]DAA1106

[^{11}C]DAA1106 (26–55 MBq) was injected into rats via tail vein under diethyl ether anesthesia. Thirty minutes after the injection, rats were sacrificed by decapitation. Brains were immediately removed and frozen in powdered dry ice. The frozen brain was cut into 40-μm thick sagittal or transaxial sections using a cryotome (HM560; Carl Zeiss, Germany). The sections were then dried under warm blowing air and contacted to an imaging plate (Fuji Film, Japan) for 2 h. The imaging plate data was analyzed by BAS1800 II system (Fuji Film). Regions of interest (ROIs) were placed on the olfactory bulb, pons/medulla, cerebellum, hippocampus, striatum, thalamus, and frontal cortex and photostimulated luminescence (PSL)/mm^2 values were used for quantification.

In vitro autoradiography of [^{11}C]DAA1106

The frozen rat brain was cut into 20-μm thick sagittal sections with a cryotome (HM560; Carl Zeiss) at −15°C. The sections were mounted on glass slides (Matsunami Glass, Japan) and stored in a deep-freezer (−80°C). The brain sections were preincubated in 50 mM Tris-HCl buffer (pH 7.4, room temperature) for 15 min, then incubated in 50 mM Tris-HCl buffer (pH 7.4, 25°C) with [^{11}C]DAA1106 (74 MBq/l, about 0.5 nM) for 60 min. After incubation they were rinsed with ice-cold Tris-HCl buffer for 2 min twice, and finally dipped into ice-cold water for 10 sec. The autoradiograms were obtained by similar procedures as for the above-mentioned ex vivo autoradiography. Nonspecific binding of [^{11}C]DAA1106 was determined by incubation in the presence of 10 μM of DAA1106.

The ratio of total binding (specific binding plus nonspecific binding) relative to the frontal cortex was used as a relative index of the ex vivo and in vitro bindings because it was difficult to keep the same injection dose (mol) of [^{11}C]DAA1106 in every experiment. The regional differences of the six brain regions and lesioned hippocampus were evaluated by one-way ANOVA. Correlation between ex vivo and in vitro [^{11}C]DAA1106 binding in the same region was evaluated by the coefficient of determination (r^2) by linear correlation.

Monkey PET study

Flumazenil (Anexate, Yamanouchi Pharmaceutical, Japan) and PK11195 (Tocris Cookson, UK) were purchased. Both DAA1106 and PK11195 were dissolved in propylene glycol with 20% ethanol. Each drug was slowly injected just before tracer injection via the tibial vein for 2 min. [^{11}C]DAA1106 was injected 5 min after drug treatment. Drug treatments were separated by at least a 2-week intervals.

All PET scans were performed using a high-resolution SHR-7700 PET camera (Hamamatsu Photonics, Japan) designed for laboratory animals, which provides 31 transaxial slices 3.6 mm (center-to-center) apart, a 33.1 cm field of view, and spatial resolution of 2.6 mm FWHM (Watanabe et al., 1997). The monkey was repeatedly anesthetized with ketamine at 10 mg/kg/hr i.m. (Ketalar, Sankyo, Japan) every hour throughout the session and immobilized with a head fixation device to ensure accuracy of repositioning (Maeda et al., 2003.). After transmission scans for attenuation correction using a ^{68}Ge-^{68}Ga source for 30 min, a dynamic emission scan in 3D acquisition mode was performed for 90 min (1 min × 4 scans, 2 min × 8 scans, 5 min × 8 scans, 10 min × 3 scans). The injected doses of [^{11}C]DAA1106 were 90.6 ± 9.3 MBq (mean ± S.D.).

After i.v. administration of [^{11}C]DAA1106, arterial blood was collected at 10, 20, and 45 sec, 1, 1.5, 2, 3, 4, 5, 6, 8, 10, 15, 20, 25, 30, 45, 60, 75, and 90 min after tracer injection. The radioactivities of whole blood samples (1.0 ml) and plasma samples were measured with a well-type γ-scintillation counter. The plasma samples were centrifuged at 15,000 rpm for 1 min at 4°C. Radioactivity was corrected for decay.

Plasma samples (250 μl) at 2, 10, 30, 60, and 90 min after tracer injection were collected in a test tube containing CH_3CN (500 μl), stirred for 15 sec, and centrifuged at 15,000 rpm for 1 min for deproteinization. An aliquot of the supernatant (100–500 μl) was injected into the HPLC system with column CAPCELL PAK C18 φ 4.6mm × 250 mm (Shiseido Co. LTD, Tokyo) and a highly sensitive positron detector under the mobile phase of CH_3CN/H_2O (1:1) at a flow rate of 2.0 ml/min. Unchanged [^{11}C]DAA1106 (t_R = 10.6 min) to the total radioactivity (corrected for decay) from the HPLC chromatogram was calculated as % = [(radioactive peak area for unchanged [^{11}C]DAA1106 /total radioactive peak area) × 100].

All emission scan images were reconstructed with a 4.0 mm Colsher filter and circular ROIs of 4-mm diameter were placed on the occipital cortex, frontal cortex, and cerebellum using image analysis software with reference to the MR image of monkey brain (in-house software PET Analyzer for Windows; Maeda et al., 2003). The uptake was expressed as the percent of injected dose per volume (% dose/ml) or the percent of maximum uptake and plotted against time. PET data from one monkey was analyzed by a three-compartment kinetics model using PMOD (PMOD Technologies, Switzerland), and k_1, k_2, k_3/k_4, and distribution volume (DV) were determined. The radioactivity in arterial plasma with metabolite and decay-corrected was used for reference.

RESULTS

First we evaluated the [^{11}C]DAA1106 binding ex vivo or in vitro by autoradiography in rats. Figure 2A shows the ex vivo and in vitro autoradiograms of rat brain with [^{11}C]DAA1106. Background count from seven

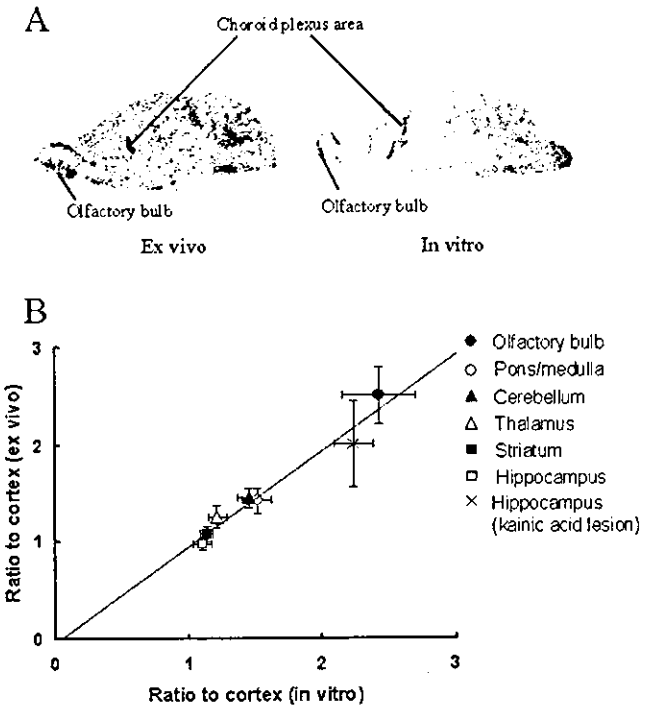

Fig. 2. **A:** Ex vivo (left panel) and in vitro (right panel) autoradiograms of [^{11}C]DAA1106 of rat brain. **B:** Linear regression between ex vivo and in vitro ratio of PSL/mm^2 value relative to the frontal cortex in 6 brain regions—olfactory bulb, pons/medulla, cerebellum, thalamus, normal or lesioned hippocampus, and striatum. Significant correlation was obtained between ex vivo and in vitro [^{11}C]DAA1106 binding. Data are presented as mean value of the PSL/mm^2 ratio to the frontal cortex ± SEM.

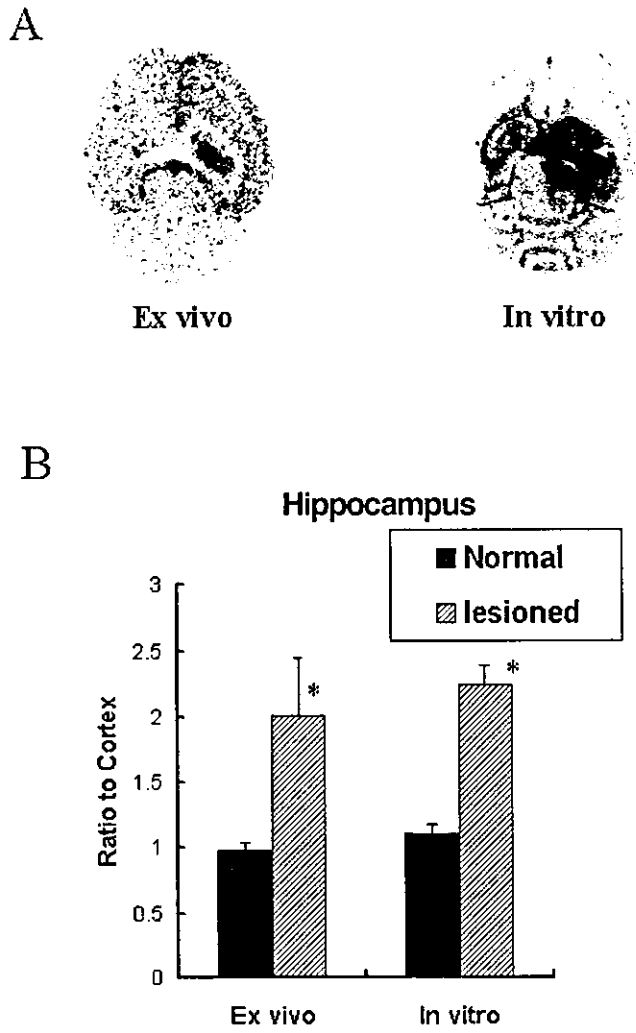

Fig. 3. **A:** Ex vivo and in vitro autoradiograms of [^{11}C]DAA1106 binding in the unilateral destruction of the dorsal hippocampus produced by kainic acid (10 nmol). The arrow indicates kainic acid-injected side. **B:** The [^{11}C]DAA1106 binding (ratio to cortex) in the normal and lesioned hippocampus ex vivo and in vitro. Closed and hatched columns represent normal and lesioned hippocampus, respectively. The destruction of hippocampus neurons was 2.0-fold higher than in the normal hippocampus in both autoradiograms.

films was 0.91 ± 0.19 PSL/mm^2 (mean ± SD). The PSL/mm^2 levels in the brain were at least 20-fold higher than the background level (data not shown). A significant regional difference was observed both ex vivo ($F_{(6,46)} = 8.9$, $P < 0.01$) and in vitro ($F_{(6,41)} = 15.7$, $P < 0.01$). The highest binding was observed in the olfactory bulb, followed by the pons/medulla and cerebellum, the frontal cortex, and hippocampus both ex vivo and in vitro. The relative binding in the olfactory bulb was significantly higher than in the other five brain regions ($P < 0.01$). The relative [^{11}C]DAA1106 binding in the cortex ex vivo correlated well with that in vitro (slope function = 0.996, $r^2 = 0.96$, $P < 0.001$; Fig. 2B). High uptake was also observed in the choroid plexus area, particularly ex vivo (Fig. 2A, left panel). In the presence of 10 μM of unlabeled DAA1106 or PK11195, cortical [^{11}C]DAA1106 binding was reduced by 70% compared to control binding (data not shown). This result suggested that specific binding of [^{11}C]DAA1106 occupies 30% of the total binding in the cortex.

Figure 3 shows the increase of hippocampal [^{11}C]DAA1106 binding ex vivo and in vitro produced by kainic acid. The rats were treated with kainic acid (10 nmol) into the right hippocampus (Fig. 3A) and the binding was evaluated at 7 days after the infusion. The ratio to the cortex value of [^{11}C]DAA1106 binding in the lesioned hippocampus was increased 2-fold compared to that in the normal hippocampus of in vitro binding [$F_{(1,11)} = 52.89$, $P < 0.001$] (Fig. 3B, right columns). This increment of [^{11}C]DAA1106 binding was similar to that of [^{11}C]PK11195 binding in the ischemic cortex of rat (Cremer et al., 1992). The ratio of specific binding of [^{11}C]DAA1106 in the lesioned hippocampus to that in the cortex was 5.4 ± 0.7 in vitro (data not shown). A significant increase of [^{11}C]DAA1106 binding by kainic acid was also observed in the ex vivo condition [$F_{(1,11)} = 8.75$, $P < 0.05$] (Fig. 3B, left columns). The magnification correlated well between ex vivo and in vitro (Fig. 2B).

To investigate the detailed brain kinetics of [^{11}C]DAA1106, we carried out PET scans using one

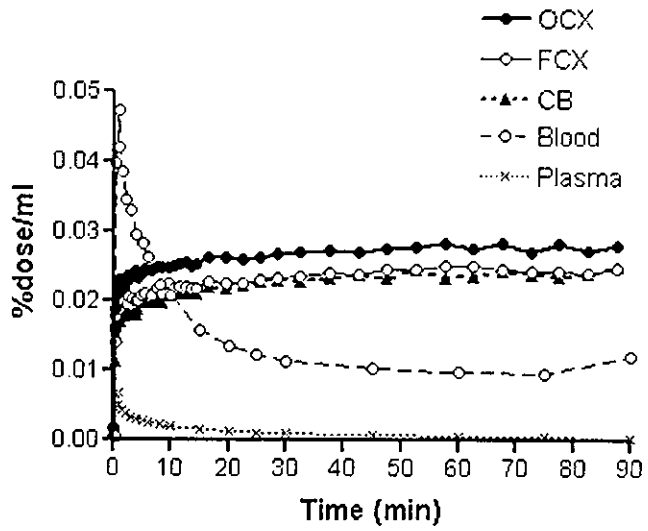

Fig. 4. Time–activity curve of [11C]DAA1106 of the monkey in the occipital cortex, frontal cortex, cerebellum, whole blood, and plasma. Radioactivity in plasma was corrected with unchanged [11C]DAA1106. The half-life of [11C]DAA1106 in plasma was estimated as 13.6 min.

rhesus monkey. The time–activity curves of [11C]DAA1106 in the monkey brain, whole blood, and plasma are shown in Figure 4. [11C]DAA1106 rapidly went into the brain and remained at almost the same uptake level during the scan time of 90 min in all measured brain regions. Radioactivity in the occipital cortex was slightly higher than that in the frontal cortex and cerebellum. The radioactivity in the occipital cortex was evaluated by three-compartment model analysis. The calculated parameters were 5.9 for k_1, 0.9 for k_2, 69.4 for DV, and 10.9 for k_3/k_4. The plasma half-life of unchanged [11C]DAA1106 was estimated as 13.6 min (data not shown). The main metabolite was considered to be only DAA1123, a precursor of [11C]DAA1106 (Zhang et al., 2003).

Figure 5A shows the summation images of [11C]DAA1106 and [11C]PK11195 in monkey brain. The accumulation of [11C]DAA1106 in the occipital cortex was slightly higher than in other brain structures, while obvious accumulation of [11C]PK11195 was not observed. The time–activity curves of [11C]DAA1106 and [11C]PK11195 in the occipital cortex are shown in Figure 5B. Radioactivity was adjusted to the injected dose (%dose/ml). The initial uptake of [11C]PK11195 decreased rapidly, whereas the initial uptake of [11C]DAA1106 remained at almost the same level for 90 min. The radioactivity of [11C]DAA1106 in the occipital cortex at 30 min after tracer injection was four times higher compared to that of [11C]PK11195. To compare the lipophilicity of [11C]PK11195 with [11C]DAA1106, we determined the logP between phosphate buffer (pH 7.4) and octanol. The logP for [11C]PK11195 was 2.7, 10-fold lower than the 3.7 for [11C]DAA1106 (Zhang et al., 2003).

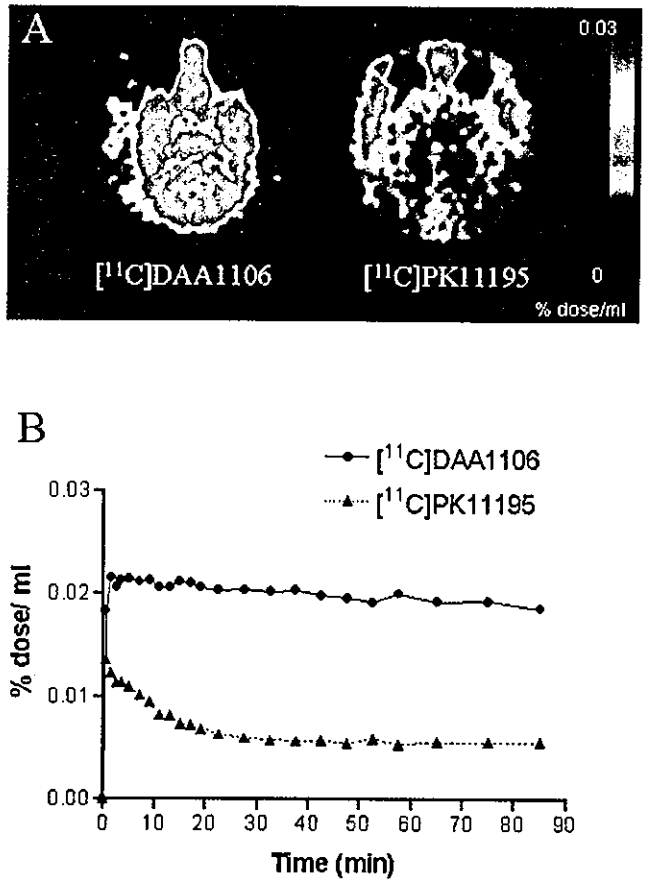

Fig. 5. **A:** Summation images (0–90 min) of [11C]DAA1106 (left panel) and [11C]PK11195 (right panel) from the brain of the same rhesus monkey. **B:** Time–activity curves of [11C]DAA1106 and [11C]PK11195 in the occipital cortex. Data were normalized to the percent of injected dose (%dose) per volume (ml). The radioactivity of [11C]DAA1106 was four times higher than that of [11C]PK11195 from 30 min after the injection.

We determined whether the [11C]DAA1106 binding in monkey brain corresponded to specific binding for PBR. Figure 6A shows the effect of pretreatment with DAA1106 (0.5 and 1 mg/kg) or PK11195 (5 and 10 mg/kg) on [11C]DAA1106 binding in the occipital cortex. Each drug was administered 5 min before tracer injection. The uptake of [11C]DAA1106 in the occipital cortex was dose-dependently decreased by DAA1106. PK11195 also inhibited the uptake of [11C]DAA1106, but there was no clear dose dependency between 5 mg/kg and 10 mg/kg. There was a marked increase in the initial uptake of [11C]DAA1106 by both DAA1106 and PK11195 pretreatment. On the other hand, flumazenil (0.1 mg/kg, i.v.) did not affect the uptake of [11C]DAA1106. Similar inhibition was obtained in the frontal cortex (Fig. 6B). Since treatment with PBR ligand increased the initial uptake of radioactivity of [11C]DAA1106, the time–activity curves were normalized to the initial peak (Fig. 6C, D). The uptake of [11C]DAA1106 was inhibited by 1 mg/kg of DAA1106 or 10 mg/kg of PK11195 to 20 or 30% of the control uptake, respectively.

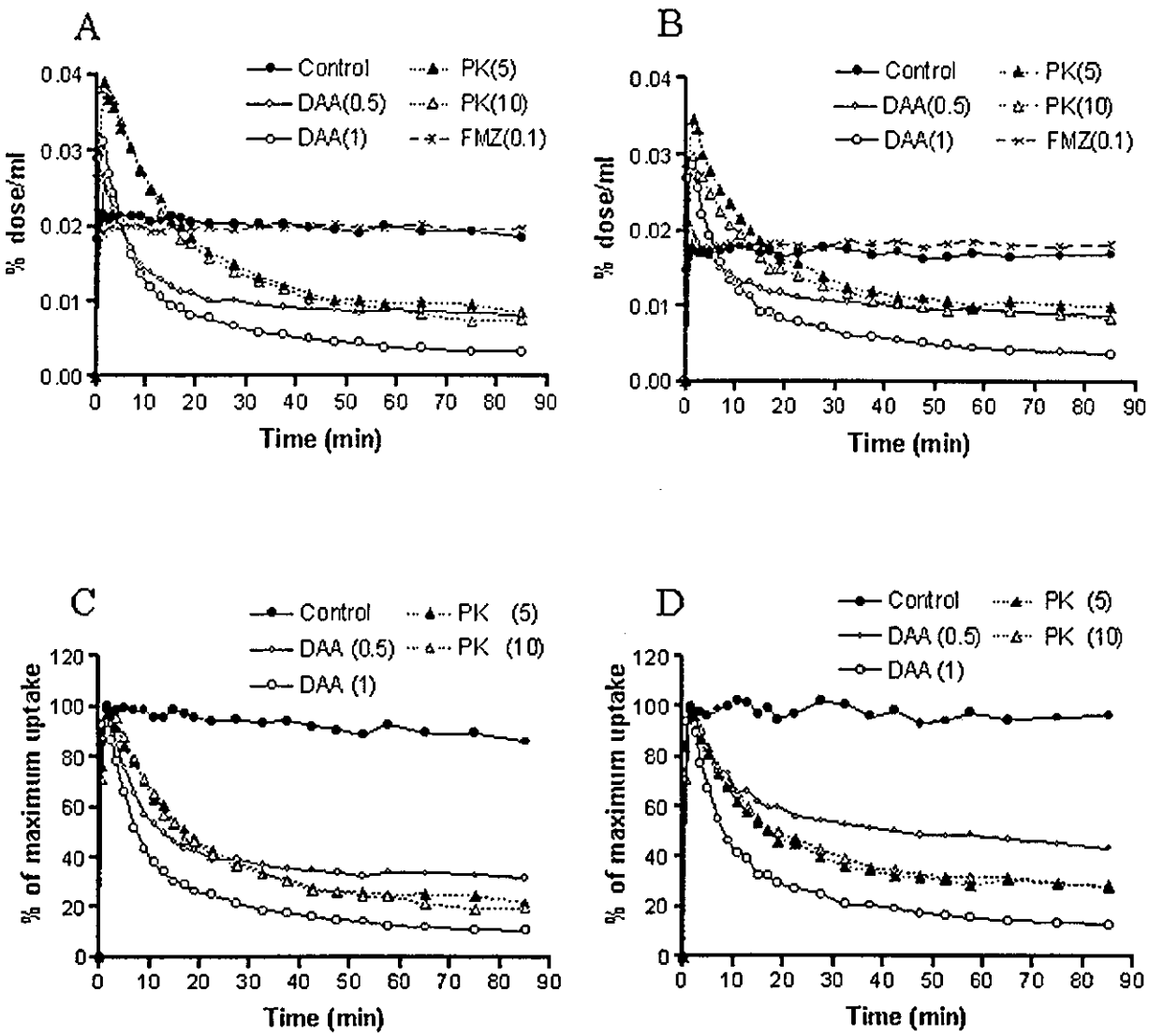

Fig. 6. **A:** The effect of drugs with affinity to PBRs or to central benzodiazepine on [^{11}C]DAA1106 binding in the occipital cortex of the monkey. The uptake was expressed as the percent of injection dose per volume (% dose/ml). The uptake of [^{11}C]DAA1106 in the occipital cortex was dose-dependently decreased by DAA1106. PK11195 also inhibited the uptake of [^{11}C]DAA1106, but without distinct dose dependency between 5 mg/kg and 10 mg/kg. There was an increase in the initial uptake of [^{11}C]DAA1106 by both DAA1106 and PK11195 pretreatment. On the other hand, flumazenil (0.1 mg/kg, i.v.) did not affect the uptake of [^{11}C]DAA1106. **B:** The effect of treatment with PBR ligands or flumazenil on [^{11}C]DAA1106 binding in the frontal cortex of the monkey. **C:** Data in the occipital (**A**) cortex are normalized to the initial maximum uptake of tracer as 100%. The uptake of [^{11}C]DAA1106 was inhibited by 1 mg/kg of DAA1106 and 10 mg/kg of PK11195 to 18% and 33% of the control uptake, respectively. **D:** Data in the frontal cortex (**B**) are normalized to the initial maximum uptake of tracer as 100%. The uptake of [^{11}C]DAA1106 was inhibited by 1 mg/kg of DAA1106 and 10 mg/kg of PK11195 to 20% and 39% of the control uptake, respectively.

The [^{11}C]DAA1106 binding seemed to be irreversible due to the slow elimination from brain. We demonstrated by in vivo displacement test whether [^{11}C]DAA1106 binding could behave in a reversible manner. The [^{11}C]DAA1106 binding was displaced by i.v. treatment with DAA1106 (1 mg/kg) or PK11195 (5 mg/kg) 30 min after tracer injection (Fig. 7).

DISCUSSION

The present results show that [^{11}C]DAA1106 had high specific binding for PBRs in the brain ex vivo as well as in vitro. The ex vivo binding of [^{11}C]DAA1106 correlated well with in vitro binding (Fig. 2B). The distribution of [^{11}C]DAA1106 in the rat brain was consistent with previous in vitro autoradiography studies using [^{3}H]Ro5-4864 (Anholt et al., 1984; Cymerman et al., 1986) and [^{3}H]PK11195 (Benavides et al., 1983). [^{11}C]DAA1106 binding in the rat brain was highest in the olfactory bulb, while that in the monkey brain was highest in the occipital cortex. The relatively higher accumulation of [^{11}C]DAA1106 in the occipital cortex was similar to the in vitro binding of [^{3}H]Ro5-4864 and [^{3}H]PK11195 in the primate brain (Cymerman et al., 1986; Rao and Butterworth, 1997).

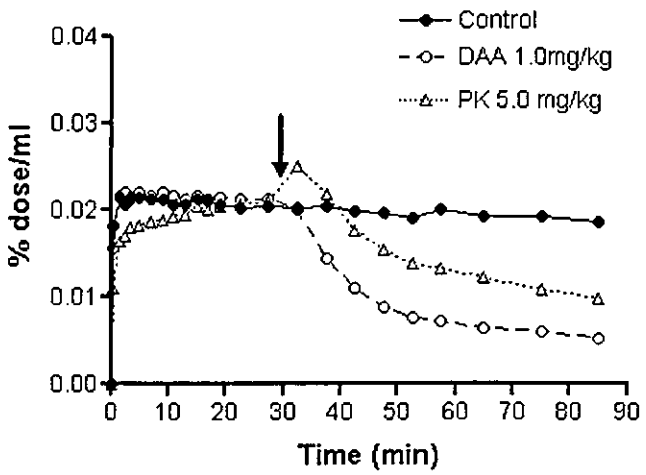

Fig. 7. Displacement of [11C]DAA1106 binding by DAA1106 (1 mg/kg) and PK11195 (5 mg/kg) in the occipital cortex of the monkey. Treatment with each drug was carried out 30 min after tracer injection (solid arrow). The uptake was expressed as the percent of injection dose per volume (% dose/ml).

The uptake of [11C]DAA1106 was markedly decreased by pretreatment with 1.0 mg/kg of DAA1106 or 10 mg/kg of PK11195, despite initial increases in uptake. We expected that the decrement of [11C]DAA1106 uptake by 1.0 mg/kg of DAA1106 was about 80% of total radioactivity, corresponding to the specific binding in vivo. The increase of initial uptake by pretreatments with DAA1106 and PK11195 can be explained by precluded [11C]DAA1106 from the peripheral organs, since the accumulation of [11C]DAA1106 (Zhang et al., 2003) and [3H]PK11195 (Hashimoto et al., 1989) is highest in the mouse lung, and the accumulation of [3H]PK11195 was completely blocked by unlabeled PBR compound (Hashimoto et al., 1989). Similar cases have been reported with [11C]PK11195 (Petit-Taboué et al., 1991) and serotonin transporter ligand [11C]cyanoimipramine (Suhara et al., 1998).

The time–activity curve of [11C]DAA1106 was analyzed by a three-compartment model. The value of k_3/k_4 reflects the slow dissociation from the binding site in the monkey brain. However, [11C]DAA1106 binding was clearly displaced by PBR ligand at 30 min after the tracer injection (Fig. 7), and our preliminary human experiment showed a clear decline in the time–activity curve of [11C]DAA1106 in the brain during the PET experiment (unpubl. obs.).

The uptake of [11C]DAA1106 in the monkey brain at 30 min was about four times higher than that of [11C]PK11195. The dissociation constant (K_d) of DAA1106 in rat brain was 10-fold smaller than that of PK 11195 (Culty et al., 2001). LogP values were 3.7 for DAA1106 (Zhang et al., 2003) and 2.7 for PK11195, indicating a lipophilicity of DAA1106 10-fold higher than that of PK11195. This difference in lipophilicity and affinity may partially explain the higher permeability and slower kinetics of DAA1106 in the brain compared to PK11195. In addition, the mechanism of the kinetic difference can be explained by the excretion from the brain through P-glycoprotein, an efflux transporter for multiple drugs, since its substrates are expected to show fast kinetics independent of its pharmacological properties (Passchier et al., 2000). PK11195 was reported to be a potent substrate of P-glycoprotein in tumor cells with multidrug resistance (Jakubikova et al., 2002). Although it is unknown whether DAA1106 is a substrate for P-glycoprotein, DAA1106 may not be excreted by P-glycoprotein due to the slow elimination from the brain.

PK11195 has weaker potency in inhibition to the [11C]DAA1106 binding than DAA1106 itself (Fig. 6). The difference in brain kinetics between DAA1106 and PK11195 suggested an insufficient amount of PK11195 in the brain. Another cause might be the heterogeneity of the ligand-binding domain on PBR. The binding domain for isoquinoline derivatives such as PK11195 was demonstrated to be on IBP (Doble et al., 1987; Riond et al., 1991), while the benzodiazepine-binding domain is thought to be on both IBP and VDAC (Garnier et al., 1994). B_{max} and K_d of DAA1106 binding for recombinant PBR in bacteria were similar to those of PK11195 binding, despite the lack of VDAC (Culty et al., 2001), and PK11195 fully displaced the [3H]DAA1106 binding (Chaki et al., 1999; Culty et al., 2001). Thus, the binding sites for both PK11195 and DAA1106 were located on IBP. However, a high concentration of PK11195 was required to displace the [3H]DAA1106 binding. This suggested that the binding domain for DAA1106 would contain an extra component that does not interact efficiently with PK11195 (Chaki et al., 1999; Culty et al., 2001).

In the present study using kainic acid, the specific binding of [11C]DAA1106 in the dorsal hippocampus was 5-fold higher than in the frontal cortex in vitro. Previous in vitro reports using [3H]PK11195 and [3H]Ro5-4864 demonstrated 3–5-fold increases in specific binding by the infusion of kainic acid (Benavides et al., 1987; Dubois et al., 1988). The microinjection of kainic acid into the brain was reported to increase the number of glial cells (Marty et al., 1991). Microglia and astrocytes were reported to be susceptible to neural destruction by kainic acid (Murabe et al., 1982; Marty et al., 1991; Dusart et al., 1991). Kuhlmann and Guilarte (2002) reported that increased [3H]PK11195 binding induced by trimethyltin corresponded to both activated microglia and proliferated astrocyte. Although activated microglia were observed after 2 days, astrocytosis was observed after 14 days. Since our experiment was evaluated at 7 days after kainic acid injection, the increased PBR binding might mainly correspond to the activated microglia.

The mechanism of neural injury-increased PBR binding can be explained by some inflammatory reactions. The activated microglia produce neuroinflamma-

tion around the damaged regions due to ablation of neural debris. Inflammatory enzymes and mediators such as phospholipase A_2, tumor necrosis factor $\alpha 1$, and interleukin-1 were reported to increase PBR binding in brain and cell culture (Havoundjian et al., 1986; Bourdiol et al., 1991; Oh et al., 1992; Rey et al., 2000). Interestingly, reactive oxygen species (ROS) generated from mitochondria polymerize few molecules of IBP through a residue of tyrosine (Delavoie et al., 2003). The polymer of IBP exhibits 5-fold higher B_{max} of PK11195 binding than the monomer of IBP (Delavoie et al., 2003). These results suggest that measuring in vivo PBR binding is useful for evaluating the extent and degree of neuroinflammation following brain injuries.

In conclusion, [^{11}C]DAA1106 showed sufficient signal to allow quantitative analysis. It seems clear that [^{11}C]DAA1106 binding can be used as an index of activated microglia with a higher signal than [^{11}C]PK11195. Furthermore, recent studies have suggested that activated microglia are involved not only in neurodegeneration but also in neurotrophic action and neural plasticity (Streit, 2002; Banati, 2002a,b). Thus, the application of [^{11}C]DAA1106 can provide useful information in the diagnosis of neurodegenerative disorders and the mechanisms of glia–neuron interactions.

ACKNOWLEDGMENTS

The authors thank Dr. S. Okuyama and Dr. A. Nakazato (Taisho Pharmaceutical Co., Japan) for providing the samples (DAA1106 and DAA1123) and for useful suggestions. We thank the members of the Cyclotron Unit and Radiopharmaceutical and Radiopharmacological Section for cyclotron operation and production of radioisotopes.

REFERENCES

Anholt RR, Murphy KM, Mack GE, Snyder SH. 1984. Peripheral-type benzodiazepine receptors in the central nervous system: localization to olfactory nerves. J Neurosci 4:593–603.

Anholt RR, De Souza EB, Oster-Granite ML, Snyder SH. 1985. Peripheral-type benzodiazepine receptors: autoradiographic localization in whole-body sections of neonatal rats. J Pharmacol Exp Ther 233:517–526.

Anholt RR, Pedersen PL, De Souza EB, Snyder SH. 1986. The peripheral-type benzodiazepine receptor. Localization to the mitochondrial outer membrane. J Biol Chem 261:576–583.

Antkiewicz-Michaluk L, Guidotti A, Krueger KE. 1988a. Molecular characterization and mitochondrial density of a recognition site for peripheral-type benzodiazepine ligands. Mol Pharmacol 34:272–278.

Antkiewicz-Michaluk L, Mukhin AG, Guidotti A, Krueger KE. 1988b. Purification and characterization of a protein associated with peripheral-type benzodiazepine binding sites. J Biol Chem 263:17317–17321.

Banati RB. 2002a. Visualising microglial activation in vivo. Glia 40: 206–217.

Banati RB. 2002b. Brain plasticity and microglia: is transsynaptic glial activation in the thalamus after limb denervation linked to cortical plasticity and central sensitization? J Physiol Paris 96:289–299.

Banati RB, Myers R, Kreutzberg GW. 1997. PK (peripheral benzodiazepine)-binding sites in the CNS indicate early and discrete brain lesions: microautoradiographic detection of [^{3}H]PK11195 binding to activated microglia. J Neurocytol 26:77–82.

Banati RB, Newcombe J, Gunn RN, Cagnin A, Turkheimer F, Heppner F, Price G, Wegner F, Giovannoni G, Miller DH, Perkin GD, Smith T, Hewson AK, Bydder G, Kreutzberg GW, Jones T, Cuzner ML, Myers R. 2000. The peripheral benzodiazepine binding site in the brain in multiple sclerosis: quantitative in vivo imaging of microglia as a measure of disease activity. Brain 123:2321–2337.

Benavides J, Quarteronet D, Imbault F, Malgouris C, Uzan A, Renault C, Dubroeucq MC, Gueremy C, Le Fur G. 1983. Labelling of "peripheral-type" benzodiazepine binding sites in the rat brain by using [^{3}H]PK 11195, an isoquinoline carboxamide derivative: kinetic studies and autoradiographic localization. J Neurochem 41: 1744–1750.

Benavides J, Fage D, Carter C, Scatton B. 1987. Peripheral type benzodiazepine binding sites are a sensitive indirect index of neuronal damage. Brain Res 421:167–172.

Bourdiol F, Toulmond S, Serrano A, Benavides J, Scatton B. 1991. Increase in omega 3 (peripheral type benzodiazepine) binding sites in the rat cortex and striatum after local injection of interleukin-1, tumour necrosis factor-alpha and lipopolysaccharide. Brain Res 543:194–200.

Braestrup C, Squires RF. 1977. Specific benzodiazepine receptors in rat brain characterized by high-affinity [^{3}H]diazepam binding. Proc Natl Acad Sci USA 74:3805–3809.

Caggiano AO, Brunjes PC. 1993. Microglia and the developing olfactory bulb. Neuroscience 52:717–724.

Cagnin A, Brooks DJ, Kennedy AM, Gunn RN, Myers R, Turkheimer FE, Jones T, Banati RB. 2001. In-vivo measurement of activated microglia in dementia. Lancet 358:461–467.

Casellas P, Galiegue S, Basile AS. 2002. Peripheral benzodiazepine receptors and mitochondrial function. Neurochem Int 40:475–486.

Chaki S, Funakoshi T, Yoshikawa R, Okuyama S, Okubo T, Nakazato A, Nagamine M, Tomisawa K. 1999. Binding characteristics of [^{3}H]DAA1106, a novel and selective ligand for peripheral benzodiazepine receptors. Eur J Pharmacol 1999 371:197–204.

Cremer JE, Hume SP, Cullen BM, Myers R, Manjil LG, Turton DR, Luthra SK, Bateman DM, Pike VW. 1992. The distribution of radioactivity in brains of rats given [N-methyl-^{11}C]PK 11195 in vivo after induction of a cortical ischaemic lesion. Int J Rad Appl Instrum B 19:159–166.

Culty M, Silver P, Nakazato A, Gazouli M, Li H, Muramatsu M, Okuyama S, Papadopoulos V. 2001. Peripheral benzodiazepine receptor binding properties and effects on steroid synthesis of two new phenoxyphenyl-acetamide derivatives, DAA1097 and DAA1106. Drug Dev Res 52:475–484.

Cymerman U, Pazos A, Palacios JM. 1986. Evidence for species differences in 'peripheral' benzodiazepine receptors: an autoradiographic study. Neurosci Lett 66:153–158.

Debruyne JC, Van Laere KJ, Versijpt J, De Vos F, Eng JK, Strijckmans K, Santens P, Achten E, Slegers G, Korf J, Dierckx RA, De Reuck JL. 2002. Semiquantification of the peripheral-type benzodiazepine ligand [^{11}C]PK11195 in normal human brain and application in multiple sclerosis patients. Acta Neurol Belg 102:127–135.

Delavoie F, Li H, Hardwick M, Robert JC, Giatzakis C, Péranzi G, Yao ZX, Maccario J, Lacapère JJ, Papadopoulos V. 2003. In vivo and in vitro peripheral-type benzodiazepine receptor polymerization: functional significance in drug ligand and cholesterol binding. Biochemistry 42:4506–4519.

Doble A, Ferris O, Burgevin MC, Menager J, Uzan A, Dubroeucq MC, Renault C, Gueremy C, Le Fur G. 1987. Photoaffinity labeling of peripheral-type benzodiazepine-binding sites. Mol Pharmacol 31: 42–49.

Dubois A, Benavides J, Peny B, Duverger D, Fage D, Gotti B, MacKenzie ET, Scatton B. 1988. Imaging of primary and remote ischaemic and excitotoxic brain lesions. An autoradiographic study of peripheral type benzodiazepine binding sites in the rat and cat. Brain Res 445:77–90.

Dusart I, Marty S, Peschanski M. 1991. Glial changes following an excitotoxic lesion in the CNS. II. Astrocytes. Neuroscience 45:541–549.

Garnier M, Dimchev AB, Boujrad N, Price JM, Musto NA, Papadopoulos V. 1994. In vitro reconstitution of a functional peripheral-type benzodiazepine receptor from mouse Leydig tumor cells. Mol Pharmacol 45:201–211.

Gavish M, Bachman I, Shoukrun R, Katz Y, Veenman L, Weisinger G, Weizman A. 1999. Enigma of the peripheral benzodiazepine receptor. Pharmacol Rev 51:629–650.

Goerres GW, Revesz T, Duncan J, Banati RB. 2001. Imaging cerebral vasculitis in refractory epilepsy using [^{11}C](R)-PK11195 positron emission tomography. AJR Am J Roentgenol 176:1016–1018.

Hashimoto K, Inoue O, Suzuki K, Yamasaki T, Kojima M. 1989. Synthesis and evaluation of ^{11}C-PK 11195 for in vivo study of peripheral-type benzodiazepine receptors using positron emission tomography. Ann Nucl Med 3:63–71.

Havoundjian H, Cohen RM, Paul SM, Skolnick P. 1986. Differential sensitivity of "central" and "peripheral" type benzodiazepine receptors to phospholipase A_2. J Neurochem 46:804–811.

Jakubikova J, Duraj J, Hunakova L, Chorvath B, Sedlak J. 2002. PK11195, an isoquinoline carboxamide ligand of the mitochondrial benzodiazepine receptor, increased drug uptake and facilitated drug-induced apoptosis in human multidrug-resistant leukemia cells in vitro. Neoplasma 49:231–236.

Jayakumar AR, Panickar KS, Norenberg MD. 2002. Effects on free radical generation by ligands of the peripheral benzodiazepine receptor in cultured neural cells. J Neurochem 83:1226–1234.

Kuhlmann AC, Guilarte TR. 2000. Cellular and subcellular localization of peripheral benzodiazepine receptors after trimethyltin neurotoxicity. J Neurochem 74:1694–1704.

Le Fur G, Perrier ML, Vaucher N, Imbault F, Flamier A, Benavides J, Uzan A, Renault C, Dubroeucq MC, Gueremy C. 1983. Peripheral benzodiazepine binding sites: effect of PK 11195, 1-(2-chlorophenyl)-N-methyl-N-(1-methylpropyl)-3-isoquinolinecarboxamide. I. In vitro studies. Life Sci 32:1839–1847.

Li H, Yao Z, Degenhardt B, Teper G, Papadopoulos V. 2001. Cholesterol binding at the cholesterol recognition/interaction amino acid consensus (CRAC) of the peripheral-type benzodiazepine receptor and inhibition of steroidogenesis by an HIV TAT-CRAC peptide. Proc Natl Acad Sci USA 98:1267–1272.

Maeda J, Suhara T, Kawabe K, Okauchi T, Obayashi S, Hojo J, Suzuki K. 2003. Visualization of α5 subunit of $GABA_A$/benzodiazepine receptor by [^{11}C]Ro15-4513 using positron emission tomography. Synapse 47:200–208.

Marty S, Dusart I, Peschanski M. 1991. Glial changes following an excitotoxic lesion in the CNS. I. Microglia/macrophages. Neuroscience 45:529–539.

McEnery MW, Snowman AM, Trifiletti RR, Snyder SH. 1992. Isolation of the mitochondrial benzodiazepine receptor: association with the voltage-dependent anion channel and the adenine nucleotide carrier. Proc Natl Acad Sci USA 89:3170–3174.

Murabe Y, Ibata Y, Sano Y. 1981. Morphological studies on neuroglia. III. Macrophage response and "microgliocytosis" in kainic acid-induced lesions. Cell Tissue Res 218:75–86.

Myers R, Manjil LG, Cullen BM, Price GW, Frackowiak RS, Cremer JE. 1991. Macrophage and astrocyte populations in relation to [^{3}H]PK 11195 binding in rat cerebral cortex following a local ischaemic lesion. J Cereb Blood Flow Metab 11:314–322.

Oh YJ, Francis JW, Markelonis GJ, Oh TH. 1992. Interleukin-1-beta and tumor necrosis factor-alpha increase peripheral-type benzodiazepine binding sites in cultured polygonal astrocytes. J Neurochem 58:2131–2138.

Okubo T, Yoshikawa R, Chaki S, Okuyama S, Nakazato A. 2004. Design, synthesis and structure-affinity relationships of aryloxyanilide derivatives as novel peripheral benzodiazepine receptor ligands. Bioorg Med Chem 12:423–438.

Okuyama S, Chaki S, Yoshikawa R, Ogawa S, Suzuki Y, Okubo T, Nakazato A, Nagamine M, Tomisawa K. 1999. Neuropharmacological profile of peripheral benzodiazepine receptor agonists, DAA1097 and DAA1106. Life Sci 64:1455–1464.

Pappata S, Levasseur M, Gunn RN, Myers R, Crouzel C, Syrota A, Jones T, Kreutzberg GW, Banati RB. 2000. Thalamic microglial activation in ischemic stroke detected in vivo by PET and [^{11}C]PK11195. Neurology 55:1052–1054.

Parola AL, Stump DG, Pepperl DJ, Krueger KE, Regan JW, Laird HE II. Cloning and expression of a pharmacologically unique bovine peripheral-type benzodiazepine receptor isoquinoline binding protein. J Biol Chem 266:14082–14087.

Passchier J, van Waarde A, Doze P, Elsinga PH, Vaalburg W. 2000. Influence of P-glycoprotein on brain uptake of [^{18}F]MPPF in rats. Eur J Pharmacol 407:273–280.

Petit-Taboué MC, Baron JC, Barré L, Travère JM, Speckel D, Camsonne R, MacKenzie ET. 1991. Brain kinetics and specific binding of [^{11}C]PK 11195 to ω3 sites in baboons: positron emission tomography study. Eur J Pharmacol 200:347–351.

Rao VL, Butterworth RF. 1997. Characterization of binding sites for the omega3 receptor ligands [^{3}H]PK11195 and [^{3}H]RO5-4864 in human brain. Eur J Pharmacol 340:89–99.

Rey C, Mauduit C, Naureils O, Benahmed M, Louisot P, Gasnier F. 2000. Up-regulation of mitochondrial peripheral benzodiazepine receptor expression by tumor necrosis factor alpha in testicular leydig cells. Possible involvement in cell survival. Biochem Pharmacol 60:1639–1646.

Riond J, Leplatois P, Laurent P, Le Fur G, Caput D, Loison G, Ferrara P. 1991. Expression and pharmacological characterization of the human peripheral-type benzodiazepine receptor in yeast. Eur J Pharmacol 208:307–312.

Schoemaker H, Bliss M, Yamamura HI. 1981. Specific high-affinity saturable binding of [^{3}H] Ro5-4864 to benzodiazepine binding sites in the rat cerebral cortex. Eur J Pharmacol 71:173–175

Schoemaker H, Boles RG, Horst WD, Yamamura HI. 1983. Specific high-affinity binding sites for [^{3}H]Ro 5-4864 in rat brain and kidney. J Pharmacol Exp Ther 225:61–69.

Sprengel R, Werner P, Seeburg PH, Mukhin AG, Santi MR, Grayson DR, Guidotti A, Krueger KE. 1989. Molecular cloning and expression of cDNA encoding a peripheral-type benzodiazepine receptor. J Biol Chem 264:20415–20421.

Squires RF, Braestrup C. 1977. Benzodiazepine receptors in rat brain. Nature 266:732–734.

Stephenson DT, Schober DA, Smalstig EB, Mincy RE, Gehlert DR, Clemens JA. 1995. Peripheral benzodiazepine receptors are colocalized with activated microglia following transient global forebrain ischemia in the rat. J Neurosci 15:5263–5274.

Streit WJ. 2002. Microglia as neuroprotective, immunocompetent cells of the CNS. Glia 40:133–139.

Suhara T, Sudo Y, Yoshida K, Okubo Y, Fukuda H, Obata T, Yoshikawa K, Suzuki K, Sasaki Y. 1998. Lung as reservoir for antidepressants in pharmacokinetic drug interactions. Lancet 351:332–335.

Watanabe M, Okada H, Shimizu K, Omura T, Yoshikawa E, Kosugi T, Mori S, Yamashita T. 1997. A high resolution animal PET scanner using compact PS-PMT detectors. IEEE Trans Nucl Sci 44:1277–1282.

Zhang MR, Tsuchiyama A, Haradahira T, Furutsuka K, Yoshida Y, Kida T, Noguchi J, Irie T, Suzuki K. 2002. Synthesis and preliminary evaluation of [^{18}F]FEtP4A, a promising PET tracer for mapping acetylcholinesterase in vivo. Nucl Med Biol 29:463–468.

Zhang MR, Kida T, Noguchi J, Furutsuka K, Maeda J, Suhara T, Suzuki K. 2003. [^{11}C]DAA1106: radiosynthesis and in vivo binding to peripheral benzodiazepine receptors in mouse brain. Nucl Med Biol 30:513–519.

Available online at www.sciencedirect.com
SCIENCE DIRECT®
International Journal of Pharmaceutics 281 (2004) 25–33
international journal of pharmaceutics
www.elsevier.com/locate/ijpharm

Factors governing the in vivo tissue uptake of transferrin-coupled polyethylene glycol liposomes in vivo

Hiroto Hatakeyama[a,1], Hidetaka Akita[a,1], Kazuo Maruyama[b], Tetsuya Suhara[c,1], Hideyoshi Harashima[a,*,1]

[a] *Laboratory for Molecular Design of Pharmaceutics, Graduate School of Pharmaceutics, Hokkaido University, Sapporo, Hokkaido 060-0812, Japan*
[b] *Faculty of the Pharmaceutical Sciences, Teikyo University, Sagamiko, Tsukui-gun, Kanagawa 199-0195, Japan*
[c] *National Institute of Radiological Sciences, 4-9-1, Anagawa, Inage-ku, Chiba-Shi, 263-8555, Japan*

Received 6 March 2004; received in revised form 24 April 2004; accepted 15 May 2004

Abstract

Liposomes, coated with transferrin (Tf)-coupled polyethylene glycol are considered to be potent carriers for drug delivery to various organs via receptor-mediated endocytosis. Since Tf receptors were ubiquitously expressed in various organs, additional perturbation of the liposomes such as regulation of the size may be required to exhibit the tissue selectivity. In the present study, the effect of size on the uptake of transferrin-coupled polyethylene glycol liposomes (Tf-PEG-L) to various organs was investigated. In liver and brain, Tf-dependent uptake was found to be dependent on the size of the liposomes used. In small liposomes with a diameter of 60–80 nm, Tf-PEG-L was taken up to these organs more efficiently than PEG-L. This Tf-dependent uptake for small liposomes decreased by the high dose administration, suggested that Tf-PEG-L is taken up via Tf receptor-mediated endocytosis even under the physiological condition, in which plasma concentration of endogenous Tf remains high. On the other hand, Tf receptor-mediated uptake was also observed in the heart, but size-dependency was not observed in this case. Collectively, these results indicate that size dependency in the uptake of Tf-PEG-L is tissue-dependent and therefore, controlling the size of Tf-PEG-L may be useful for the success of tissue targeting.

Keywords: Transferrin; Liposomes; Receptor-mediated endocytosis; Tissue uptake

1. Introduction

Liposomes coated with polyethyleneglycol (PEG-L) have shed light on their use as potent drug carriers, since these have the ability to escape from the reticuloendothelial system (RES) and to circulate in the blood for a long period (Blume and Cevc, 1990; Klibanov et al., 1990; Allen and Hansen, 1991; Klibanov et al., 1991; Mori et al., 1991; Litzinger et al., 1994; Maruyama et al., 1999). In addition, various ligands or antibodies can be further attached to the surface-granted PEG chains, thus permitting them to be actively taken up by the target cells via receptor-mediated endocytosis (Maruyama et al., 1999). One example is transferrin (Tf), whose receptors are ubiquitously expressed in various tissues including the luminal membrane of the brain capillary endothelium, and tumor cells have also been used for targeting (Ponka and Lok, 1999; Qian et al., 2002). Pardridge

* Corresponding author. Tel.: +81-11-706-3919; fax: +81-11-706-4879.
E-mail address: harasima@pharm.hokudai.ac.jp (H. Harashima).
[1] Advanced and Innovational Research Program in Life Sciences.

0378-5173/$ – see front matter © 2004 Elsevier B.V. All rights reserved.
doi:10.1016/j.ijpharm.2004.05.025

and co-workers developed immunoliposomes against this receptor, and succeeded in the delivery of anticancer drugs (e.g. doxorubicin), oligo DNA and plasmid DNA to the brain via receptor-mediated transcytosis (Liu et al., 1992; Huwyler et al., 1996, 1997; Pardridge, 1999; Lee et al., 2000, 2002a,b; Shi et al., 2000, 2001; Shi and Pardridge, 2000).

In addition, Ishida et al. (2001) demonstrated the utility of Tf-coupled PEG liposomes (Tf-PEG-L) for the intracellular targeting of the liposomes to tumor cells via receptor-mediated endocytosis. They also showed that small liposomes with a diameter of 60 nm were taken up by tumor cells by receptor-mediated endocytosis, but not those of 120 nm. Considering that the majority of the coated vesicles were less than 100 nm (Steven et al., 1983), sizing of ligand-coupling PEG liposomes that are below this threshold is also essential for successful intracellular targeting. To investigate whether this rule can be also applied to normal tissues, we kinetically evaluated the uptake of differently sized PEG-L and Tf-PEG-L. In the present study, we raise finding that size dependency in the uptake of Tf-PEG-L is tissue-dependent and therefore, regulation of the size of liposomes may lead to the tissue targeting.

2. Materials and methods

2.1. Materials

Cholesterol (CH) and distearoyl-*sn*-Glycero-3-phoshoethanolamine-*N*-[methoxy (polyethylene glycol)-2000] (DSPE-PEG) were purchased from Avanti Polar Lipids, Inc. (Alabaster, AL). DSPE-PEG with a functional maleimide moiety at the terminal end of PEG: *N*-[(3-maleimide-1-oxopropyl)aminopropyl polyethyleneglycol-carbamyl] distearoylphosphatidylethanolamine (DSPE-PEG-Mal) and egg phosphatidylcholine (EPC) were purchased from Nippon Oil and Fat Co. (Tokyo, Japan). [cholesteryl-1,2-3H(*N*)]-cholesteryl hexadecyl ether ([^{3}H]CHE) and [^{3}H]inulin was purchased from Perkin-Elmer Life Science Japan (Tokyo, Japan). Human holo-Tf and 3-(2-pyridyldithiopropionic acid *N*-hydroxy-succimide ester (SPDP) were purchased from Sigma (St. Louis, MO). Male ddy mice (5–6 weeks old) were purchased from Sankyo Labo Service (Sapporo, Japan).

2.2. Preparation of PEG-L and Tf-PEG-L

PEG-L was prepared from EPC, CH, and DSPE-PEG in a molar ratio of 2:1:0.18. [^{3}H]CHE and [^{3}H]inulin were used as a lipid phase marker and an aqueous phase marker, respectively. Different sizes of liposomes were prepared by a reverse phase evaporation method, followed by extrusion with an Avanti Mini-Extruder. To prepare large liposomes with a size of 140–180 nm, liposomes were extruded through polycarbonate membrane filters (pore size of 0.2 μm) 19 times. To prepare small liposomes with a size of 60–80 nm, large liposomes were further extruded through polycarbonate membrane filters having pore size of 0.1 and 0.05 μm for 19 times each. The distribution of liposome diameter was determined by a dynamic laser scattering method with an ELS-8000HO instrument (Otsuka Electronics, Osaka, Japan).

Concerning the Tf-PEG-L, EPC, CH, DSPE-PEG and DSPE-PEG-Mal were first mixed at molar ratios of 2:1:0.15:0.03, and liposomes were prepared, as described above. Prior to this, Tf was modified with SPDP. A 20 mM solution of SPDP in methanol was reacted with the Tf (approximately 60 nmol), dissolved in PBS (pH 7.4) by stirred for 30 min at room temperature. The product was purified by chromatography on Sephadex G25. Dithiothleitol (DTT) was then added to the Tf-SPDP, at a final concentration of 50 mM, followed by 30 min incubation in the dark, to reduce the SPDP to permit it to react with the maleimide moiety on the surface of the PEG-liposome. After the separation of the product using Sephadex G25, the reduced Tf was incubated with the liposomes over night at 4 °C. Tf-PEG-L was separated from the free Tf by Bio-Gel A1.5m (BioRad: Hercules, CA). Recovery of the liposomes and Tf was evaluated by a cholesterol *E*-test WAKO (Wako: Osaka, Japan) and a BCA protein assay kit (Pierce: Rockford, IL), respectively. Small and large liposomes would be expected to contain approximately 210 and 450 molecules per liposome, respectively.

2.3. Pharmacokinetic analysis of the Tf-PEG-L and PEG-L

The liposomes were injected into a ddy mouse via the tail vein. The doses of liposomes were fixed at 2 nmol lipid/g BW (low dose) or 36 nmol lipid/g BW

(high dose). At the indicated times, the mice were sacrificed and blood, brain, liver, spleen, skeletal muscle and lung were collected. After weighing the samples, blood and organ samples were solubilized in Soluene-350 (Perkin-Elmer Life Sciences) for 5 h at 50 °C. Blood samples were decolorized by H_2O_2. The radioactivities were determined by liquid scintillation counting, after adding 10 ml of scintillation fluid (Hionic Flour; Perkin-Elmer Life Sciences).

Data analysis was performed, as described in the previous study (Harashima et al., 1992a,b). Plasma concentrations at the indicated times, $C(t)$ are expressed as %ID (injected dose) per ml of blood radioactivity (%ID/ml). Pharmacokinetic parameters were determined by fitting the $C(t)$ to a mono-exponential equation, as follows, using a non-linear regression analysis by the MULTI program:

$$C(t) = A\,e^{-kt}$$

The areas under the blood concentration–time curve (AUC) were calculated based on the following equation:

$$\mathrm{AUC} = \int_{0\,\mathrm{h}}^{48\,\mathrm{h}} C(t)\,dt = \frac{A}{k}(1 - e^{-k\times 48})$$

To clarify the distribution of liposomes in the body, the radioactivities in the various organ samples, X_{organ} were first measured (Fig. 1). However, these values included a contribution by liposomes in the vascular space as well as the tissue parenchyma (including the macrophages and the capillary endothelial cells) (X_{tissue}). Therefore, a correction was made for liposomes in the vascular space as follows:

$$X_{\mathrm{tissue}} = X_{\mathrm{organ}} - V_0 C(t)$$

where V_0 denotes the total volume of the vascular space and interstitial fluid, as determined by the radioactivities in the whole organ samples divided by the blood concentration 10 min after the i.v. injection of the [^{3}H]CHE-labeled PEG-L. Except for the liver or spleen, the capillary in other organs consisted of the continuous capillary, in which the distances of the open junction was less than 4 nm. Therefore, V_0 represents the capillary volume since paracellular capillary permeability of PEG-L is negligible. The uptake clearance (CL) in various tissues at 48 h were calculated as follows:

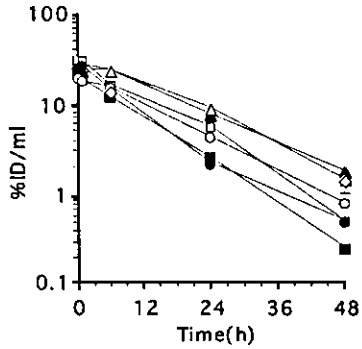

Fig. 1. Time profiles of the blood concentration of PEG-L and Tf-PEG-L. Open circles, closed circles, open squares and closed squares indicate the time profiles of the blood concentration, represented by %ID/ml of small PEG-L, small Tf-PEG-L, large PEG-L and large Tf-PEG-L, labeled with [^{3}H]CHE after the administration of a low dose (2 nmol lipid/g BW), respectively. Open and closed triangles indicate the results of small PEG-L and Tf-PEG-L after the administration of a high dose (36 nmol/g BW), respectively. Blood concentration of small PEG-L labeled liposomes with the aqueous phase marker of [^{3}H]inulin at 6 and 48 h are plotted as diamonds. Data are represented by the mean ± S.E. ($n = 3$).

$$\mathrm{CL} = \frac{X_{\mathrm{tissue}}}{\mathrm{AUC}}$$

This calculation is based on the assumption that the liposomes taken up by the organs were not effluxed to the blood in the previous report (Lee et al., 2000), and it was supported by the experimental data (Harashima et al., 1992a).

3. Results and discussion

3.1. Plasma concentration and organ distribution of the PEG-L and Tf-PEG-L

For the optimization of the ligand-directed active targeting of the liposomes, the rapid elimination due to the nonspecific uptake by the reticuloendothelial system (RES) must be avoided. To overcome this barrier, PEG chains were attached to the surface of the liposomes (Blume and Cevc, 1990; Klibanov et al., 1990, 1991; Allen and Hansen, 1991; Mori et al., 1991; Litzinger et al., 1994; Maruyama et al., 1999), and ligands were coupled to the ends of the PEG chains. It has previously been determined that the Tf-dependent uptake of liposomes to tumor tissues only occurs for

Table 1
Kinetic parameters for the blood elimination of PEG-L and Tf-PEG-L

	C_0 (%ID/ml)	k (h^{-1})	$T_{1/2}$ (h)	Total body clearance (ml/h)
PEG-L (small, low)	19.9	0.067	10.3	9.72
Tf-PEG-L (small, low)	26.4	0.10	6.93	14.4
PEG-L (large, low)	28.4	0.078	8.90	11.2
Tf-PEG-L (large, low)	21.4	0.093	7.45	13.4
PEG-L (small, high)	31.9	0.063	10.9	9.16
Tf-PEG-L (small, high)	27.7	0.057	12.1	8.25

the small size (<60 nm), but not >120 nm liposomes (Ishida et al., 2001). This result prompted us to investigate the effect of size on the uptake of ligand-coupled PEG-L to normal tissues. In the present study, we have compared the disposition of PEG-L and Tf-PEG-L with small (the average diameter of 60–80 nm) and large (the average diameter of 140–180 nm) size.

First, time-profiles for the blood elimination of PEG-L and Tf-PEG-L labeled with [^{3}H]CHE were compared over a 48 h period (Fig. 1). As demonstrated previously (Ishida et al., 2001), Tf-PEG-L and PEG-L have a long circulation with a half-life of >6 h, and the total clearances of these liposomes are comparable irregardless of size (Table 1). This suggests that modulation with Tf did not affect the RES uptake process. Furthermore, blood concentrations of PEG-L labeled with [^{3}H]CHE were compared to an encapsulating membrane-impermeable aqueous phase marker, [^{3}H]inulin in order to verify that the liposomes are intact even 48 h after i.v. administration. If [^{3}H]inulin were released from disintegrated liposomes, it would be rapidly eliminated from the body with a half-life of <5 min (data not shown). Therefore, [^{3}H]inulin that was not associated with liposomes had no effect on the blood concentration of the [^{3}H]inulin-labeled PEG-L. Since the encapsulation ratio of [^{3}H]inulin to the liposomes was limited, we injected [^{3}H]inulin-labeled PEG-L at a high dose (36 nmol lipid/g BW) to permit the detection of radioactivity, even at 48 h. As shown in Fig. 1, the blood concentrations of the [^{3}H]inulin-labeled liposomes at 6 and 48 h were comparable to the [^{3}H]CHE-labeled sample injected at a high dose, suggesting that the liposomes remained intact even at 48 h.

Organ distributions (X_{organ}) of PEG-L and Tf-PEG-L in the liver, spleen, lung, heart, skeletal muscle and brain were then evaluated 48 h after i.v. administration (Fig. 2). As shown previously, a large portion of the liposomes were recovered from the liver and spleen (>5% ID/g organ), suggesting that these are major clearance organs even for long circulating liposomes (Liu et al., 1992; Litzinger et al., 1994; Maruyama et al., 1999). As shown in the case of the tumor tissues, paracellular permeability partially contributes to the passive accumulation. In addition, active uptake mechanisms such as phagocytosis by Kupper cells in the liver, or filtration by a meshwork consisting of reticular fibers and accompanying macrophages in the red pulp in spleen can be attributed to these high clearances, as reported previously (Klibanov et al., 1991; Litzinger et al., 1994). The uptake of the large PEG-L in spleen was further enhanced compared with small liposomes, presumably because large liposomes were efficiently trapped by filtration, as shown previously (Klibanov et al., 1991; Liu et al., 1992; Litzinger et al., 1994). Following these organs, lung, heart and muscle showed relatively high X_{organ} values (>0.5% ID/g tissue), while the brain was much lower (<0.1% ID/g tissue). It is generally thought that the blood brain barrier, constituting of the tight junction between the adjacent endothelial cells severely interrupts the movement of small molecules (Gloor et al., 2001; Huber et al., 2001; Wolburg and Lippoldt, 2002). Therefore, the extent of organ distribution of liposomes is presumably dependent on their permeability through the gap of the endothelial cells.

The uptake of liposomes from the blood to the tissues was then calculated based on the data shown in Figs. 1 and 2, and represented by the CL, in which the vascular space was corrected as described in Material and Method. In these calculations, the V_0 values in liver, spleen, lung, heart, muscle and brain were determined to be 219 ± 28.5 μl/g liver, 141 ± 34 μl/g spleen, 229 ± 12 μl/g lung, 281 ± 30 μl/g heart, 19.8 ± 1.9 μl/g muscle and 20.2 ± 0.5 μl/g brain, respectively by i.v. injection of [^{3}H]CHE-labeled PEG-L. The effects of size and dose on the tissue uptake of liposomes are shown in Figs. 3 and 4. Statistical differences, determined by one-way or two-way ANOVA followed by the Student–Newman–Keuls test are also summarized in Table 2.

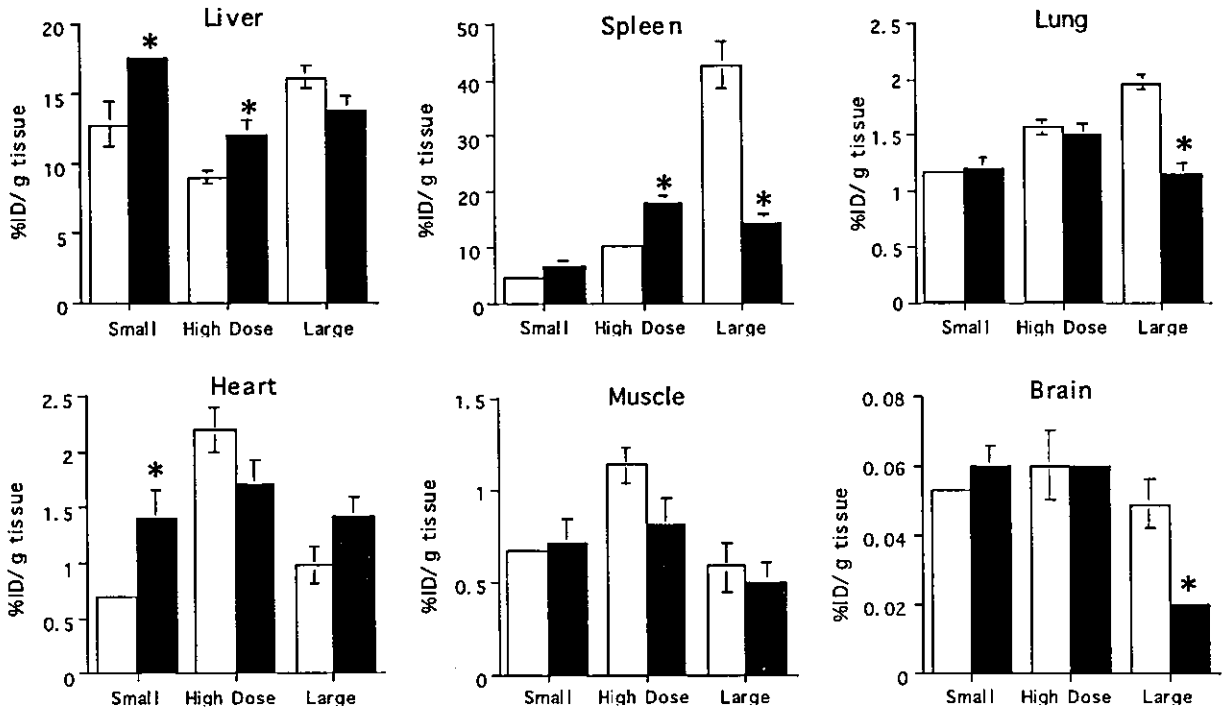

Fig. 2. The organ distribution of PEG-L and Tf-PEG-L The organ distribution was expressed as the percentage injection dose per gram of organ (%ID/g organ), in liver, spleen, lung, heart, skeletal muscle and brain at 48 h after an i.v. injection of [^{3}H]CHE labeled PEG-L and Tf-PEG-L. Open and closed bars indicate the results for PEG-L and Tf-PEG-L, respectively. Data are represented by the mean ± S.E. (n = 3). * Significantly different between PEG-L and Tf-PEG-L ($P < 0.05$ by Student's t-test).

Table 2
Summary of statistical analyses for of size- and dose-dependent-uptake of the PEG-L and Tf-PEG-L

CL (μL/h/g tissue)	Tissue	Dose[a]	Size[b]	Tf-dependent tissue[b] uptake	
				Small	Large
>20	Liver	○	×	○[c]	×
	Spleen	○	○	×	×
0.5–6	Lung	○	×	×	×
	Heart	×	×	○	○
	Muscle	×	×	×	×
0.05–0.2	Brain	○	○	○[c]	×

[a] The statistical differences of the size- and dose-dependent uptake of liposomes were determined by two-way ANOVA ((○) $P < 0.05$).

[b] The statistical differences for the transferring-dependent uptake was determined by two-way ANOVA followed by Student–Newman–Keuls test ((○) $P < 0.05$).

[c] The statistical differences for the transferring-dependent uptake was determined by one-way ANOVA followed by Student–Newman–Keuls test ((○) $P < 0.05$).

3.2. *Effect of dose on the tissue uptake of the PEG-L and Tf-PEG-L*

First, absolute values for the CL of small PEG-L injected at a low dose were compared among the various organs. Similar to the rank order of X_{organ}, values for CL were high in the liver and spleen (>15 μl/h/g tissue). As discussed above, active uptake such as entrapment by the Kupper cells in the liver and filtration by the meshwork of reticular fibers in the spleen may explain the high CL values found for the liver and spleen. With respect to the other organs, the CL value in the brain (<0.2 μl/h/g tissue) was much lower than that in the lung, heart and muscle (1–4 μl/h/g tissue). Considering that the CL values were significantly reduced in various organs such as liver, lung and brain (Fig. 3 and Table 2), active uptake such as phagocytosis by the macrophages, or pinocytosis by the endothelial cells and/or tissue parenchyma may be involved.

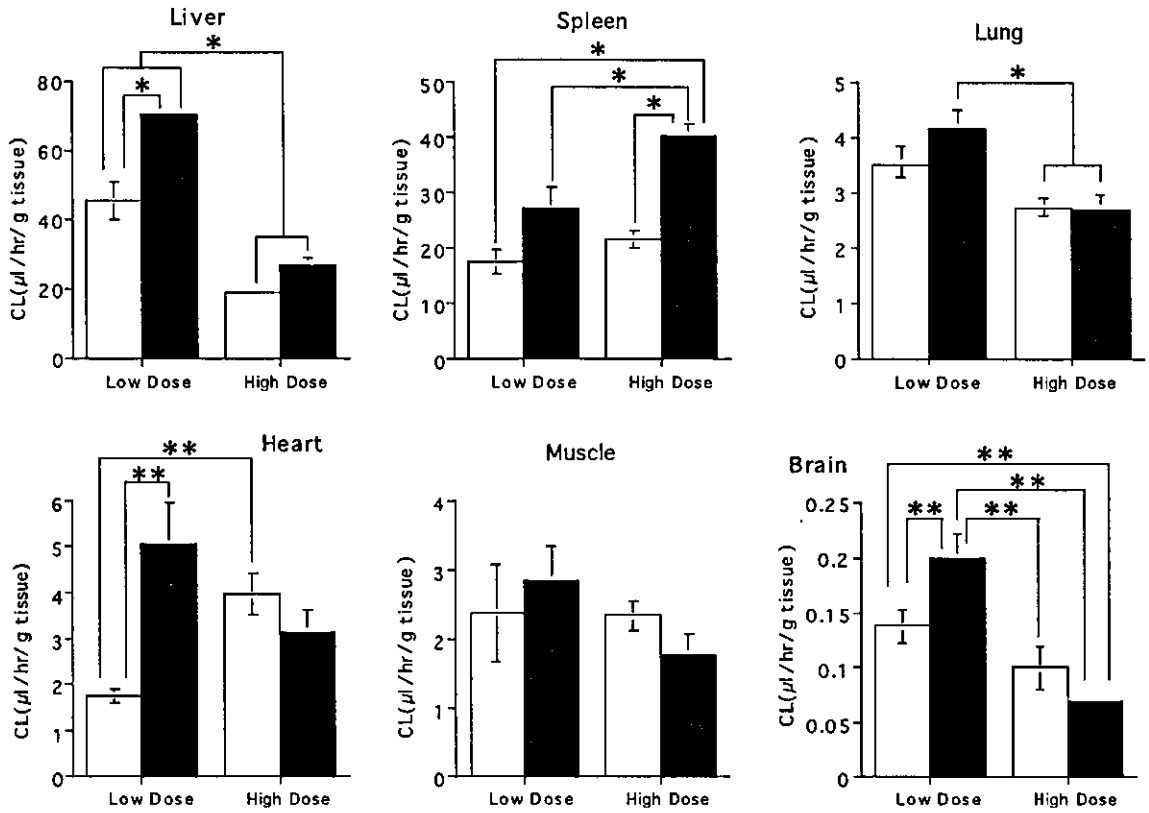

Fig. 3. Effect of liposomes dose on the uptake clearances A comparison of the tissue uptake clearance by the various organs between a low dose injection (2 nmol lipid/g BW) and a high dose injection (36 nmol lipid/g BW). The uptake clearances for the small PEG-L (open bars) and Tf-PEG-L (closed bars) were calculated using the data in Figs. 1 and 2, as described in Section 2. Open and closed bars indicated results for PEG-L and Tf-PEG-L, respectively. Data are represented by mean ± S.E. ($n = 3$). * Significantly different between PEG-L and Tf-PEG-L ($P < 0.05$ by two-way ANOVA, followed by Student–Newman–Keuls test). ** Significantly different between PEG-L and Tf-PEG-L ($P < 0.05$ by one-way ANOVA, followed by Student–Newman–Keuls test).

Then, the effect of the modulation of Tf was investigated. Considering that endogenous plasma concentration of Tf (approximately 10 μM) is significantly higher than Kd values of Tf receptor (approximately 1 nM), they should be saturated under the physiological condition (Klausner et al., 1983). However, in the present study, Tf-dependent uptake was observed in the liver, brain and heart at low dose injection (2 nmol lipids/g body weight), and moreover, this effect is diminished by the administration of high doses of liposomes (36 nmol lipids/g body weight), suggesting that Tf-PEG-L was taken up by Tf receptor-mediated endocytosis (Fig. 3 and Table 2). In these conditions, initial (<6 h) concentration of the liposomes injected by low dose and high dose were estimated as 12.2 and 245 μM, respectively. These values are converted to approximately 10 and 300 nM in terms of the Tf concentration modified on the Tf-PEG-L. These data can be accounted for by assuming that inhibition constant (K_i) of Tf against the Tf-PEG-L was significantly higher than Kd value of Tf receptors, since Tf-PEG-L exhibits the multivalent binding to the Tf receptors and high concentration of Tf are necessary to remove all of these binding. The values for the Tf-dependent uptake by these organs in liver (~25 μl/h/g tissue), muscle (~4 μl/h/g tissue) and brain (~0.05 μl/h/g tissue) were quite different. This can be attributed to the differences in the density of Tf-receptors or internalization rate via endocytosis among these organs. In contrast, the uptake of Tf-PEG-L by the spleen was drastically enhanced when a high dose was injected, presumably because

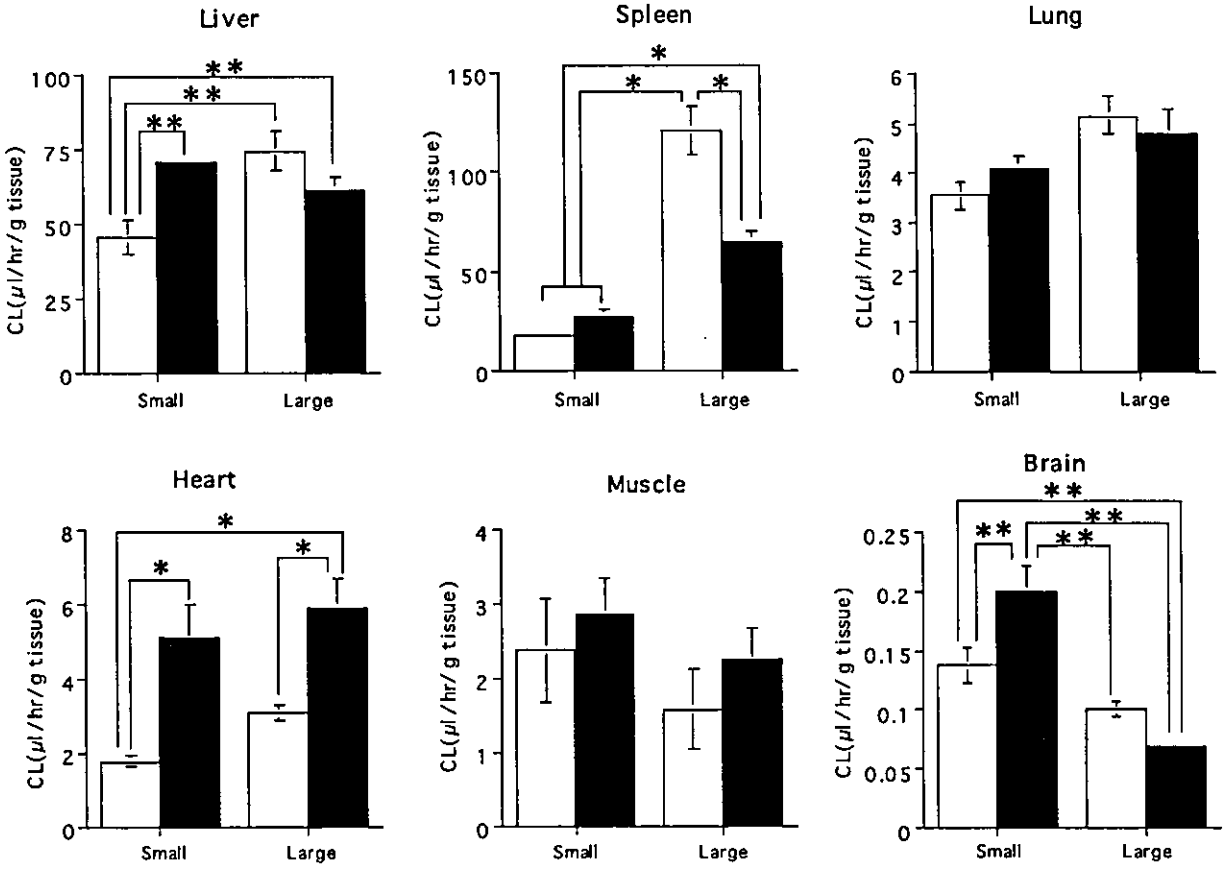

Fig. 4. Effect of liposome size on the uptake clearances. The uptake clearances of the small and large PEG-L (open bars) and Tf-PEG-L (closed bar) injected at a low dose (2 nmol lipid/g BW) were calculated using the data in Figs. 1 and 2 as described in Section 2. Open and closed bars indicate the results for PEG-L and Tf-PEG-L, respectively. Data are represented as the mean ± S.E. ($n = 3$). * Significantly different between PEG-L and Tf-PEG-L ($P < 0.05$ by two-way ANOVA, followed by Student–Newman–Keuls test). ** Significantly different between PEG-L and Tf-PEG-L ($P < 0.05$ by one-way ANOVA, followed by Student–Newman–Keuls test).

of the immunogenesis derived from the human transferring attached to the PEG (Fig. 3 and Table 2).

On the other hand, in other organs such as lung and skeletal muscle, Tf-dependent uptake was barely detectable, in spite of the high or ubiquitous expression of Tf receptors (Ponka and Lok, 1999; Qian et al., 2002). These results are not in agreement with prior observations. It has been demonstrated that coupling of the antibody against Tf to a receptor (OX26) PEG liposomes are able to enhance accumulation by the spleen and lung in rats (Huwyler et al., 1997). Furthermore, PEG-L coupled with the OX26 monoclonal antibody is taken up by in vitro L6 cell cultures derived from skeletal muscle (Schnyder et al., 2003). In addition, when antibodies against the Tf receptor were injected into the cynomolgous monkeys, a large portion of the dose was recovered from the skeletal muscle (Friden et al., 1996). These contradictions suggest that Tf is a much less potent ligand than OX26. In fact, the absolute value for the uptake of CL by the brain was approximately 1/15 of that of OX26 coupled PEG-L in rats (Huwyler et al., 1997)

3.3. Effect of size on the tissue uptake of the PEG-L and Tf-PEG-L

Finally, the effect of size on the tissue uptake of liposomes was investigated (Fig. 4 and Table 2). In

the heart and especially the spleen, the CL values for large liposomes were significantly increased over that of small liposomes. In addition, such a size-dependent uptake was also observed in the liver (e.g. small PEG-L versus large PEG-L), although the differences were not significant by two-way ANOVA. These findings are consistent with previous observations showing that larger liposomes are more susceptible to recognition by the complement system, followed by the phagocytosis by macrophages (Harashima et al., 1996). Therefore, entrapment by macrophages partially contributes to tissue uptake in these organs. In contrast, small liposomes were more extensively taken up by the brain. Presumably, pinocytosis, rather than phagocytosis plays a role in tissue uptake in the brain.

Concerning the hepatic uptake, Tf-dependent uptake was observed only for small liposomes, whereas no or little change was detected for large ones, suggesting that uptake via receptor-mediated endocytosis functions in the uptake of small liposomes with sizes less than 60–80 nm but not for the large ones because the major part of the diameter of the coated vesicles was less than 100 nm (Steven et al., 1983). This hypothesis is also supported by the fact that adenoviruses, with a diameter of 70–90 nm are able to efficiently access the liver parenchymal cells, resulting in a high level of transgene expression (Herz and Gerard, 1993). Such a size-dependent efficiency for endocytosis in vivo is also in agreement with an in vitro study showing that the internalization of large-sized cell-associated microspheres (200 nm) is substantially slower than that of small ones (50–100 nm) (Rejman et al., 2003). A size-dependent delay in uptake was also observed in viral particles (Matlin et al., 1982) and polyplexes (Godbey et al., 1999). Similarly, the Tf-dependent uptake of the liposomes was also observed only for the small liposomes by the brain, where Tf receptors are highly expressed on the luminal membrane of the endothelial cells. The uptake of Tf-PEG-L by brain capillary endothelial cells is consistent with previously reported microscopic observations (Omori et al., 2003). The size-dependent efficiency of clathrin-mediated endocytosis, as described above, also explains this result. In contrast to the liver and brain, Tf-dependent uptake by the heart was clearly observed and was independent of the size of the liposomes (Fig. 4). Although the mechanism remains to be elucidated, smooth muscle cells in the heart may accept large particles via clathrin-coated vesicles.

4. Conclusion

In conclusion, a small size, less than 80 nm is an important factor for the tissue targeting of Tf-PEG-L based on receptor-mediated endocytosis, especially in the liver and brain. On the other hand, the heart is able to take up both small and large liposomes in a Tf-dependent manner. These results suggest that Tf can be the ligand for the active targeting of PEG-L in vivo even in the physiological condition, and regulation of size confer the tissue selectivity of Tf-PEG-L.

Acknowledgement

This study was performed through the Advanced and Innovational Research Program in Life Sciences from the Ministry of Education, Culture, Sports, Science and Technology, the Japanese Government.

References

Allen, T.M., Hansen, C., 1991. Pharmacokinetics of stealth versus conventional liposomes: effect of dose. Biochim. Biophys. Acta 1068, 133–141.

Blume, G., Cevc, G., 1990. Liposomes for the sustained drug release in vivo. Biochim. Biophys. Acta 1029, 91–97.

Friden, P.M., Olson, T.S., Obar, R., Walus, L.R., Putney, S.D., 1996. Characterization, receptor mapping and blood-brain barrier transcytosis of antibodies to the human transferrin receptor. J. Pharmacol. Exp. Ther. 278, 1491–1498.

Gloor, S.M., Wachtel, M., Bolliger, M.F., Ishihara, H., Landmann, R., Frei, K., 2001. Molecular and cellular permeability control at the blood-brain barrier. Brain Res. Rev. 36, 258–264.

Godbey, W.T., Wu, K.K., Mikos, A.G., 1999. Tracking the intracellular path of poly(ethylenimine)/DNA complexes for gene delivery. Proc. Natl. Acad. Sci. U.S.A. 96, 5177–5181.

Harashima, H., Komatsu, S., Kojima, S., Yanagi, C., Morioka, Y., Naito, M., Kiwada, H., 1996. Species difference in the disposition of liposomes among mice, rats, and rabbits: allometric relationship and species dependent hepatic uptake mechanism. Pharm. Res. 13, 1049–1054.

Harashima, H., Kume, Y., Yamane, C., Kiwada, H., 1992a. Non-Michaelis-Menten type hepatic uptake of liposomes in the rat. J. Pharm. Pharmacol. 44, 707–712.

Harashima, H., Ohshima, S., Midori, Y., Yachi, K., Kikuchi, H., Kiwada, H., 1992b. Kinetic analysis of tissue distribution of